Geological Magazine

www.cambridge.org/geo

Petrogenesis and geochemical characteristics of Plio-Quaternary alkali basalts from the Qorveh–Bijar volcanic belt, Kurdistan Province, NW Iran

Nafiseh Salehi[1], Ashraf Torkian[1], Tanya Furman[2] and Petrus le Roux[3]

[1]Department of Geology, Faculty of Science, Bu-Ali Sina University, Hamedan, Iran; [2]Department of Geosciences, Pennsylvania State University, University Park, PA, USA and [3]Department of Geological Sciences, University of Cape Town, Rondebosch 7701, South Africa

Original Article

Cite this article: Salehi N, Torkian A, Furman T, and le Roux P (2023) Petrogenesis and geochemical characteristics of Plio-Quaternary alkali basalts from the Qorveh–Bijar volcanic belt, Kurdistan Province, NW Iran. *Geological Magazine* **160**: 888–904. https://doi.org/10.1017/S0016756823000018

Received: 29 June 2022
Revised: 15 November 2022
Accepted: 1 January 2023
First published online: 17 February 2023

Keywords:
partial melting; pyroxenite; drip magmatism; isotopic data; thermobarometer; metasomatized lithosphere

Author for correspondence:
Ashraf Torkian, Email: a-torkian@basu.ac.ir

Abstract

The Pliocene–Quaternary volcanic rocks which outcrop between Qorveh and Bijar are part of post-collisional within-plate volcanic activity in northern Iran. These mafic alkaline rocks form part of the northern arm of the Sanandaj–Sirjan (Hamedan–Tabriz) zone. Thermobarometry on equilibrium clinopyroxene – whole-rock pairs yields pressures and temperatures of 4–6 (±1.8) kbar and 1182–1213 (±27) °C, respectively; olivine – whole-rock (melt) equilibrium thermometry yields crystallization temperatures of 1212–1264 (±27) °C. Field relationships, including the presence of pyroxenitic xenoliths, and geochemical evidence (e.g. high FeO/MnO, and low CaO compared to lavas derived from peridotite sources) suggest a pyroxenitic mantle source for the studied rocks. Variation of trace elements and isotopic ratios (i.e. Ce/Pb, Ba/La, $^{87}Sr/^{86}Sr$) indicate that this pyroxenite mantle source was generated by interaction between melted sediments of the subducted Neo-Tethys slab with ambient peridotitic lithospheric mantle. The resulting metasomatized lithosphere is denser and has a lower viscosity than the peridotitic mantle, and tectonic disturbance can cause it to fall into the depths of the mantle. The descending volatile-rich material starts to melt with increasing temperature. Modelling of rare earth element (REE) abundances suggests that <1 % partial melting of the descending pyroxenite could create the Plio-Quaternary alkali basaltic magma of the Qorveh–Bijar. The geochemical evidence for lithospheric foundering, and hence drip magmatism, in the Qorveh–Bijar volcanic belt is supported by seismographic studies indicating thinned lithosphere beneath the study area.

1. Introduction

Alkali basaltic magmas are observed in several tectonic environments, including intra-continental, intra-oceanic, post-collisional and arc settings (e.g. Rostami-Hossouri *et al.* 2020). Kogarko (2006) has noted that generally alkaline magmatism is most typical of stable regions where it is controlled by rift structures and occurs along zones marked by abruptly decreasing thickness of the continental lithosphere. These compositions have received considerable attention regarding their geochemistry, petrology and geodynamic evolution (Cebria *et al.* 2000; Temel *et al.* 2000, 2010; Thompson *et al.* 2005; Xu *et al.* 2005; Jung *et al.* 2006; Kuritani *et al.* 2008, 2009; Pilet *et al.* 2008; Zeng *et al.* 2011; Ducea *et al.* 2013; Pang *et al.* 2013; Torkian *et al.* 2016; Rostami-Hossouri *et al.* 2020; Salehi *et al.* 2020; Verma & Molaei-Yeganeh, 2022). The alkaline basalts parental magmas were produced by relatively small degrees of melting (<5 wt %) of their heterogeneous mantle source (Fitton & Dunlop, 1985) and, as such, alkali basalts may be taken as deep probes of enriched domains in the upper mantle (Farmer *et al.* 2002). Modern geochemical and isotopic data show that alkali–basaltic magmas are formed by melting of enriched reservoirs within the lithospheric and sub-lithospheric mantle (Thompson *et al.* 2005; Xu *et al.* 2005; Jung *et al.* 2006; Kogarko, 2006; Kogiso & Hirschmann 2006; Sobolev *et al.* 2007; Pilet *et al.* 2008; Kuritani *et al.* 2009; Zeng *et al.* 2010; Ma *et al.* 2011).

This study explores the petrogenesis of Plio-Quaternary mafic alkaline volcanic rocks that outcrop between the two cities of Qorveh and Bijar. This volcanic episode has been the subject of extensive research, which sets the stage for addressing the origin, age and tectonic settings of the volcanic rocks erupted during this period. The petrogenesis of these volcanic rocks is broadly related to subduction of Neo-Tethyan oceanic crust and continental collision (Malecootyan *et al.* 2007; Kord, 2012). Malecootyan *et al.* (2007) conclude that crustal contamination occurred during the upward movement of magma to the surface and this process was responsible for the distinct compositional characteristics (enrichment in Pb, Rb and Sr and depletion in Nb and Zr)

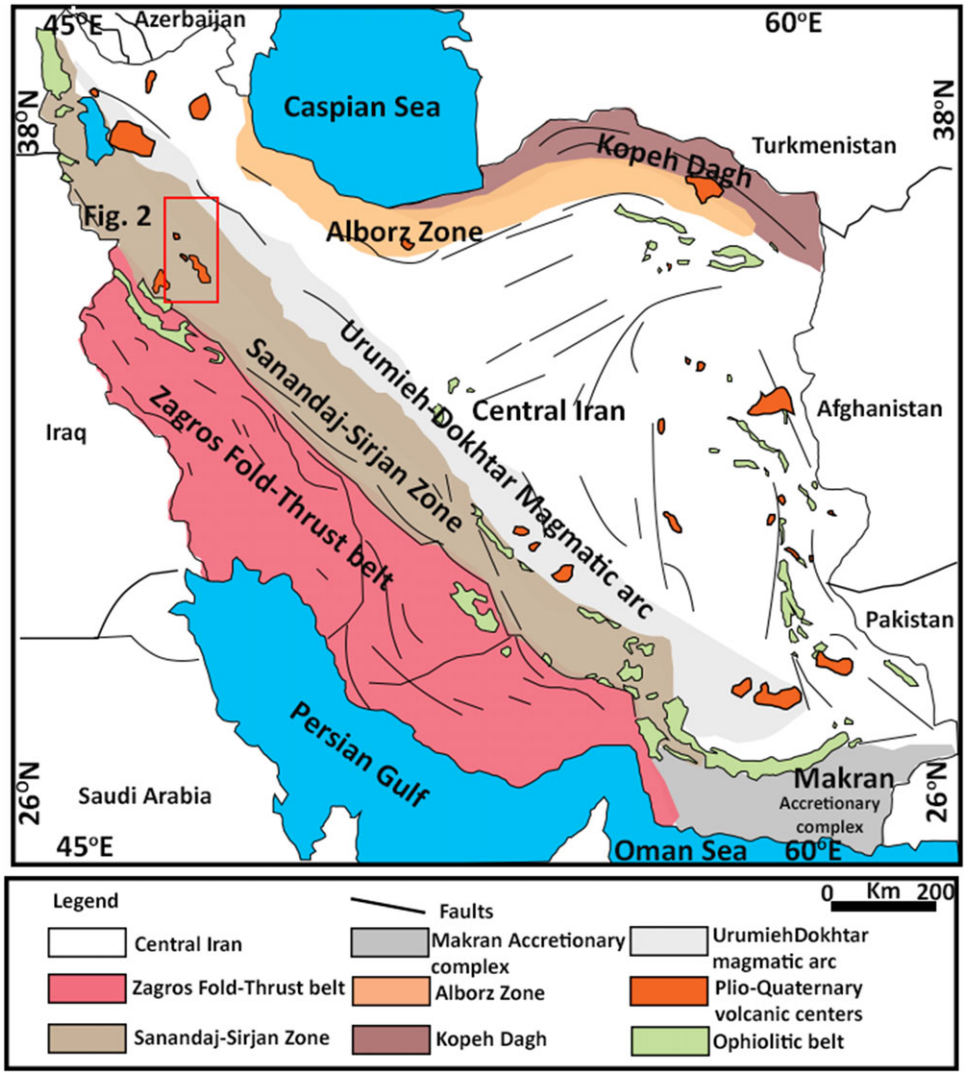

Fig. 1. (Colour online) Late Cenozoic volcanic centres and active faults in Iran. The study area is included in the red rectangle (the rectangle shows the study area from Allen *et al.* 2013).

of the Qorveh–Bijar volcanic rocks. Torkian *et al.* (2016) documented the existence of gneissic xenoliths and quartz and alkali feldspar xenocrysts in the NW Qorveh volcanic rocks as evidence of crustal contamination phenomena that may partly overprint the geochemistry of the mantle source. Several authors suggest they derived from an ocean island basalt (OIB)-like mantle source (Moinevaziri & Amin-Sobhani, 1988; Razavi & Sayyareh, 2010). Allen *et al.* (2013) suggested that the high La/Nb and Zr/Hf of the Qorveh–Bijar volcanic rocks indicates a mantle source which was affected by slab-derived fluids. The high Nb concentration and other geochemical features led Azizi *et al.* (2014) to interpret these volcanic rocks as high-Nb basalts generated by partial melting of metasomatized mantle associated with adakitic magma. Recent calculations of the parental melt composition based on olivine-hosted melt inclusions demonstrated a pyroxenite source for Quaternary alkaline (Salehi *et al.* 2020).

Here we present new interpretations based on whole-rock geochemistry (major elements, trace elements and Sr–Nd isotopes) that constrain the contribution of crustal contamination to the genesis of these rocks, as well as highlighting the possible role of subducted oceanic crust in the geochemistry of the mantle source. Detailed mineral chemistry is used to retrieve the intensive variables of the magmatic system. We integrate the petrological and geochemical information derived for the Qorveh–Bijar volcanic belt to provide additional constraints on the melting conditions of the mantle source beneath the Arabian–Eurasian collision zone.

2. Geological setting

The Cenozoic continental collision between the Iranian and Arabian plateaus is manifest in widespread magmatic and metamorphic features in Iran. The subduction of Neo-Tethyan oceanic lithosphere beneath eastern Turkey and Iran initiated during Early Jurassic or Late Triassic time (Dewey *et al.* 1973; Berberian & King, 1981; Alavi, 1994; Stampfli & Borel, 2002; Hassanzadeh & Wernicke, 2016; Barber *et al.* 2018; Tavakoli *et al.* 2020). Subsequent northward motion of the Arabian plate following final closure of Neo-Tethys occurred during the late Oligocene – early Miocene (e.g. Dewey *et al.* 1973; Berberian & King, 1981; Alavi, 1994; Mouthereau *et al.* 2012; Hassanzadeh & Wernicke, 2016; Barber *et al.* 2018; Tavakoli *et al.* 2020) or the Late Cretaceous – Oligocene (Mohajjel & Fergusson 2014). The closure of Neo-Tethys has given rise to the East Anatolian and Iranian plateaus to the north and east, respectively, of the Bitlis–Zagros suture (Fig. 1).

https://doi.org/10.1017/S0016756823000018 Published online by Cambridge University Press

There are considerable variations in the style and quantity of magmatism after the Arabia–Eurasia collision. Magmatic rocks ranging in age from Miocene to Quaternary are geographically dispersed, volumetrically modest and chemically varied. The complex continental collision zone in western Iran (Fig. 1) consists of the Zagros fold-and-thrust belt (ZFTB), the Sanandaj–Sirjan zone (SaSZ), and the Urumieh–Dokhtar magmatic belt (UDMB) (Berberian & King, 1981; Alavi, 1994; Hassanzadeh & Wernicke, 2016; Tavakoli *et al.* 2020). The SaSZ can be divided into distinct northern and southern sections (Eftekharnejad, 1981; Ghasemi & Talbot, 2006). The northern section is mainly composed of an old island arc and an active continental margin that collided in the Late Jurassic – Early Cretaceous. The southern section consists entirely of metamorphic basement with evidence of polyphase deformation and metamorphism (Azizi & Asahara, 2013). The SaSZ has been intruded by A-, S- and I-type granitoid batholiths emplaced from Jurassic to Oligocene time (e.g. Sepahi & Athari, 2006; Mansouri-Esfahani *et al.* 2010; Shahbazi *et al.* 2010; Torkian & Furman, 2015; Yeganeh *et al.* 2018).

Between the Main Zagros Thrust (MZT) in the southwest and the Tabriz Fault in the northeast, Azizi & Moinevaziri (2009) proposed a subdivision of SaSz in northwestern Iran that is of Cretaceous and Eocene–Miocene to Quaternary age, trending in a NW–SE direction and including three minor volcanic belts: (1) the Sonqor–Baneh volcanic belt (SBVB), (2) the Hamedan–Tabriz volcanic belt (HTVB) and (3) the Cretaceous volcanic belt (SCVB) (see fig. 3 in Azizi & Moinevaziri, 2009). The SCVB consists mainly of mafic to intermediate submarine volcanics of calc-alkaline affinity, and the SBVB is composed of basalt, as well as gabbro to dioritic bodies, with extrusive to sub-volcanic magmatic textures and tholeiitic to alkaline affinity.

The HTVB extends across the Hamedan to Tabriz and consists of Miocene to Plio-Quaternary extrusive rocks. The northern part of this belt has Miocene volcanic rocks with adakitic features (Azizi *et al.* 2014; Lechmann *et al.* 2018; Torkian *et al.* 2019; Shahbazi *et al.* 2021). The southern part consists of two different volcanic suites: felsic to intermediate rocks of Miocene age and Plio-Quaternary basalts (Şengör & Kidd, 1979; Kheirkhah & Mirnejad, 2014). Here we investigate mafic volcanic rocks in the HTVB located between the cities of Qorveh and Bijar (i.e. 35° 18′–35° 30′ N, 47° 46′– 47° 59′ E; Fig. 2). The results of K–Ar whole-rock dating in Qorveh–Bijar conducted by Boccaletti *et al.* (1976) suggest that the volcanic activity occurred during the Quaternary, from 1.3 ± 0.08 to 0.5 ± 0.15 Ma.

3. Field relationships

The Qorveh–Bijar volcanic products comprise bombs, scoria, lapilli tuffs and lava flows with an individual thickness up to several tens of metres (Fig. 3a, b); we refer to these units collectively as the QBB (Qorveh–Bijar basaltic rocks). Cinder cones represent the youngest phase of magmatism in the region, preserving their geological structures over the lava flows. The lava flows cover the argillaceous limestone of Miocene to Pliocene time. There is no significant deposition postdating the lava flows, and three-dimensional structures are exposed through dissection by an external drainage (Fig. 3c).

Felsic gneissic xenoliths are frequently observed in the basaltic rocks and some of these xenoliths are larger than 10 cm (Fig. 3d).

4. Material and methods

4.a. Whole-rock geochemistry

Whole-rock major and trace element contents of the studied samples were determined on glassy pills synthetized with the Pt-loop technique at 1600 °C in a chamber furnace installed at the HP-HT Laboratory of Experimental Volcanology and Geophysics of the Istituto Nazionale di Geofisica e Vulcanologia (INGV; Rome, Italy). The pills were then analysed using an electron probe microanalyser (EPMA) Jeol-JXA8200 with combined energy-dispersive spectrometry – wavelength-dispersive spectrometry (EDS-WDS; five spectrometers with 12 crystals) using 15 kV accelerating voltage and 10 nA electric current. A slightly defocused electron beam with a size of 3 μm was used, with a counting time of 5 s on background and 15 son peak. Sodium and potassium were analysed first to prevent alkali migration effects. The accuracy of the microprobe was measured through the analysis of well-characterized synthetic oxides and mineral standards. Based on counting statistics, analytical uncertainties relative to their reported concentrations indicate that precision was better than 5 % for all cations.

Trace element compositions of whole rocks were measured by laser ablation inductively coupled plasma mass spectrometry (LA-ICP-MS) conducted at the Institute of Geochemistry and Petrology of ETH Zürich (Switzerland) using a 193 nm ArF Excimer laser from Resonetic coupled to a Thermo Element XR ICP-MS. A spot size of 43 μm was used for mineral analyses and reduced to 20 μm for glass analyses; output energy of the laser beam was typically ~3.5 J cm^{-2}. NIST612 and NIST610 were adopted as external standards for the data reduction. United States Geological Survey (USGS) reference glass GSD-1G was used as a secondary standard to monitor instrument accuracy. When appropriate, major element concentrations from EPMA analyses were used as internal standards. Long-term laboratory reproducibility of homogeneous glass standards indicates precision significantly better than 5 % for elements whose concentration was much greater (i.e. ≥2×) than the detection limit.

4.b. Isotope analysis

Radiogenic isotopic data were obtained at the Department of Earth Science, University of Cape Town (South Africa). Approximately 50 mg of the powdered rock was dissolved in a 4:1 HF/HNO_3 acid mixture in sealed Savillex beakers for 48 h, and then the solution was split for determination of both concentration data (Rb, Sr, Nd and Sm), and Sr and Nd isotope ratios. The Sr and Nd fractions for isotope analyses were isolated employing sequential column chemistry (after Pin *et al.* 1994; Pin & Zalduegui, 1997; Míková & Denková, 2007). The Sr and Nd isotope data were obtained using a Nu Plasma HR mass spectrometer equipped with a DSN-100 desolating nebulizer. All Sr isotopes were referenced to a value of 0.710255 for the bracketing analyses of NIST SRM987. During the analysis, Sr isotope data were corrected for Rb interferences using the measured signal for ^{85}Rb and the natural $^{85}Rb/^{87}Rb$ ratio, while instrumental mass fractionation was addressed using the exponential law and the $^{86}Sr/^{88}Sr$ ratio of 0.1194. The Nd isotope values were normalized to 0.512115 for bracketing analyses of JNdi-1. These data were then corrected for Sm and Ce interferences using the signals measured for ^{147}Sm and ^{140}Ce and natural Sm and Ce isotope abundances, while instrumental mass fractionation was addressed using the exponential law and the $^{146}Nd/^{144}Nd$ ratio of 0.7219.

https://doi.org/10.1017/S0016756823000018 Published online by Cambridge University Press

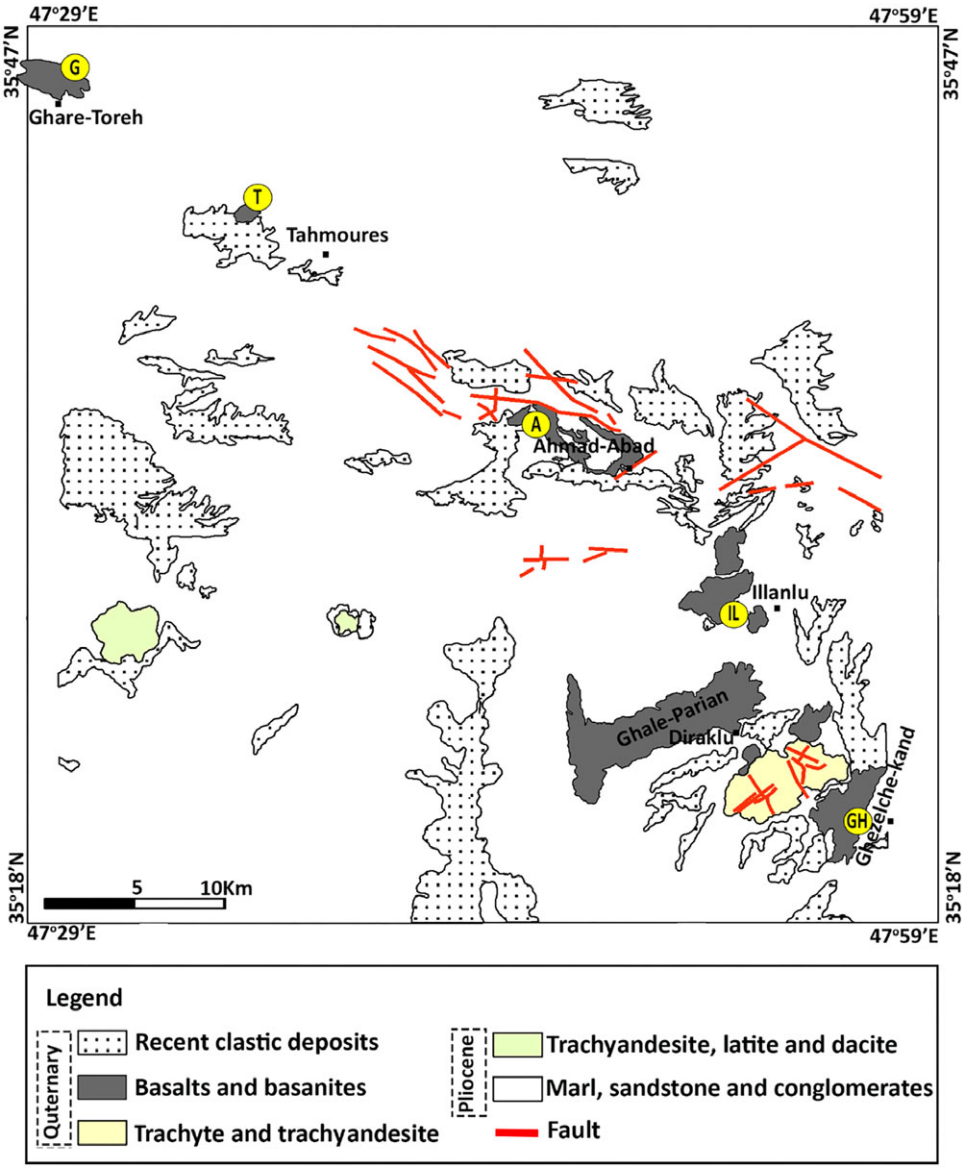

Fig. 2. (Colour online) Schematic geological map showing the location of lava flows in the study area. After Emami *et al*. (1993). The sampling sites are shown. Abbreviations in the diagram are Gh (Ghezelche-Kand), IL (Illanlu), A (Ahmad-Abad), T (Tahmoures) and G (Ghare-Toreh).

5. Results

5.a. Petrography

The studied samples are generally fresh and show porphyritic and microlithic textures (Fig. 4a–c). Phenocrysts and microphenocrysts (35–45 vol. %) are represented primarily by clinopyroxene and olivine; in some cases amphibole and biotite are present as accessory phases (Fig. 4e). The groundmass (<35 vol. %) includes microlites of clinopyroxene, acicular plagioclase and opaque minerals (titanomagnetite), all coexisting with glass (~20 vol. %). Glomeroporphyritic aggregates of olivine and clinopyroxene are observed in some samples.

5.b. Mineral chemistry

All mineral compositional data are provided in supplemental files as Tables S1 and S2 (available online at https://doi.org/10.1017/S0016756823000018). Clinopyroxene up to 2 mm is the most abundant mafic mineral phase in all studied rocks. The crystals are commonly euhedral to subhedral and display normal and oscillatory zoning. Some crystal cores and rims show sieve textures with embayments (Fig. 4d). The absence of reaction rims is considered as an indicator of equilibrium between the crystal and the host magma. The clinopyroxenes (Fig. 5a) are classified as diopside to salite with $Wo_{41.3\text{-}49.4}$, $En_{36.4\text{-}47.6}$, $Fs_{6.6\text{–}12}$, Mg# 0.40–0.89 (Mg# expressed as molar Mg/(Mg + Fe^{+2}) where iron is Fe^{2+} total). Many crystals are slightly zoned, showing increasing TiO_2 and FeO concentrations and decreasing MgO contents towards the rims (Fig. 5b, c).

Olivine is the second most abundant phenocryst phase. Crystals are euhedral to subhedral in shape, showing sporadically skeletal and glomeroporphyritic textures (Fig. 4). Some of the olivine phenocrysts display a dissolving–erosion structure, while in other cases the crystals are broken and replaced with iddingsite along fractures and rims. The forsterite content of olivine is variable (Fig. 6a) and generally decreases from core to rim following the normal growth zoning. The highest forsterite content ($Fo_{82\text{–}88}$) is measured in olivine crystals from the Illanlu area. The CaO

https://doi.org/10.1017/S0016756823000018 Published online by Cambridge University Press

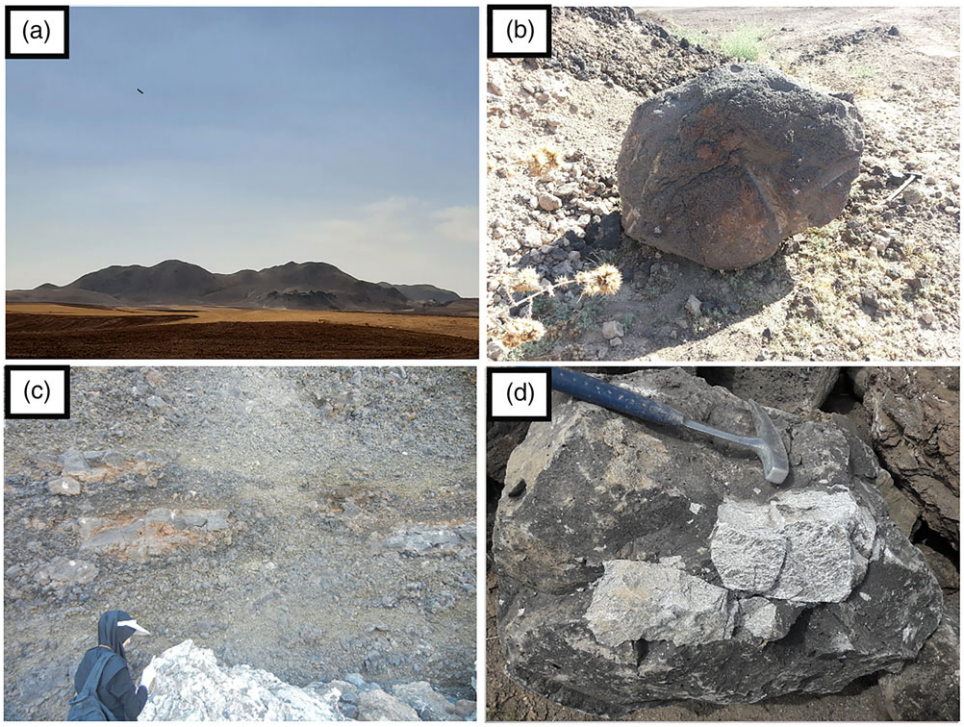

Fig. 3. (Colour online) Overview of the products object of this study. (a) Scoria cones, (b) volcanic bombs, (c) scoria and lavas and (d) gneissic xenoliths.

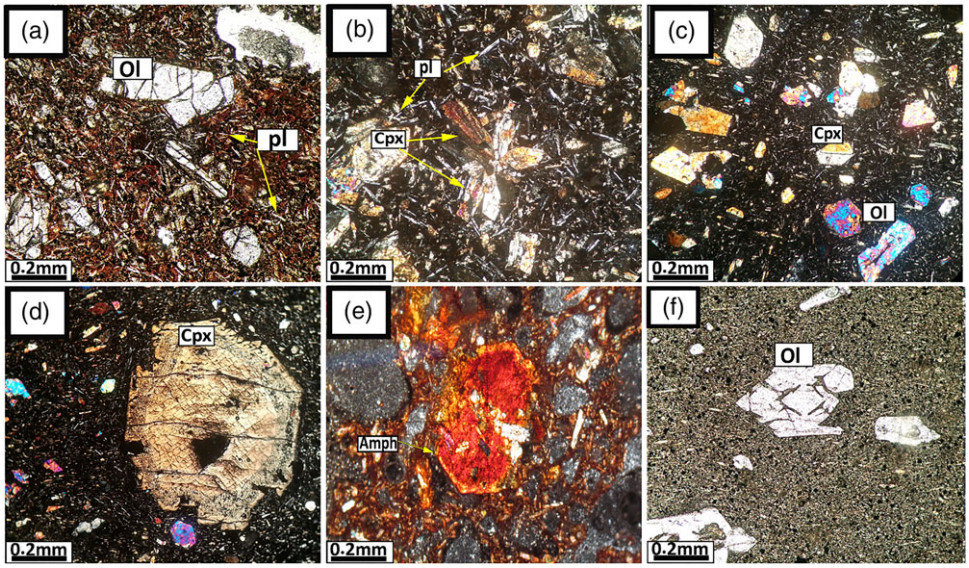

Fig. 4. (Colour online) Representative photomicrographs of the studied volcanic rocks. (a) Microlithic porphyry texture; (b) glomeroporphyry texture; (c) porphyry texture; (d) sieve texture of clinopyroxene; (e) amphibole; (f) skeletal olivine. Ol: Olivine; Cpx: Clinopyroxene; Qtz: Quartz; Bt: Biotite; Pl: Plagioclase.

content of olivine ranges from 0.16 to −2.9 wt %, which is higher than olivine from mantle xenoliths (CaO <0.1 wt %; Thompson & Gibson, 2000).

5.c. Whole-rock geochemistry

Representative whole-rock (major and trace element) compositions are given in the supplemental file as Table S3 (available online at https://doi.org/10.1017/S0016756823000018). The studied rocks are identified as basanite and phono-tephrite with alkaline affinity in a plot of total alkalis vs SiO_2 (Le Bas *et al.* 1986) (Fig. 6b); they are generally sodic with $Na_2O > 2 + K_2O$.

QBB rocks contain 45.3–48.0 wt % SiO_2, 8.1–10.3 wt % MgO, and their Mg# (Mg# = Mg/(Mg + Fe)) ranges from 65 to 72. Variations in Al_2O_3, Na_2O, K_2O and SiO_2 vs MgO do not define clear trends, and no systematic variations are found between Sr, Nb, La, Th and MgO. However, MgO contents correlate positively with CaO, Ni and Cr (Fig. 7).

Figure 8 shows the chondrite-normalized rare earth elements (REE) and the primitive-mantle-normalized trace element patterns of the QBB rocks. Similar to other intraplate alkaline basalts (Zou *et al.* 2000; Wilson & Patterson, 2001; Shaw *et al.* 2003; Aydin *et al.* 2008; Asan & Kurt, 2011; Pang *et al.* 2013), all the samples are enriched in light REE (LREE), exhibiting steep REE patterns (Fig. 8a) with $(La/Yb)_N$ values ranging from 33.1 to 68.3. The sub-parallel and tight REE patterns suggest that these volcanic rocks originated from a common mantle source. The QBB are enriched in large-ion lithophile elements (LILE) (Cs: 1.1–3.6

https://doi.org/10.1017/S0016756823000018 Published online by Cambridge University Press

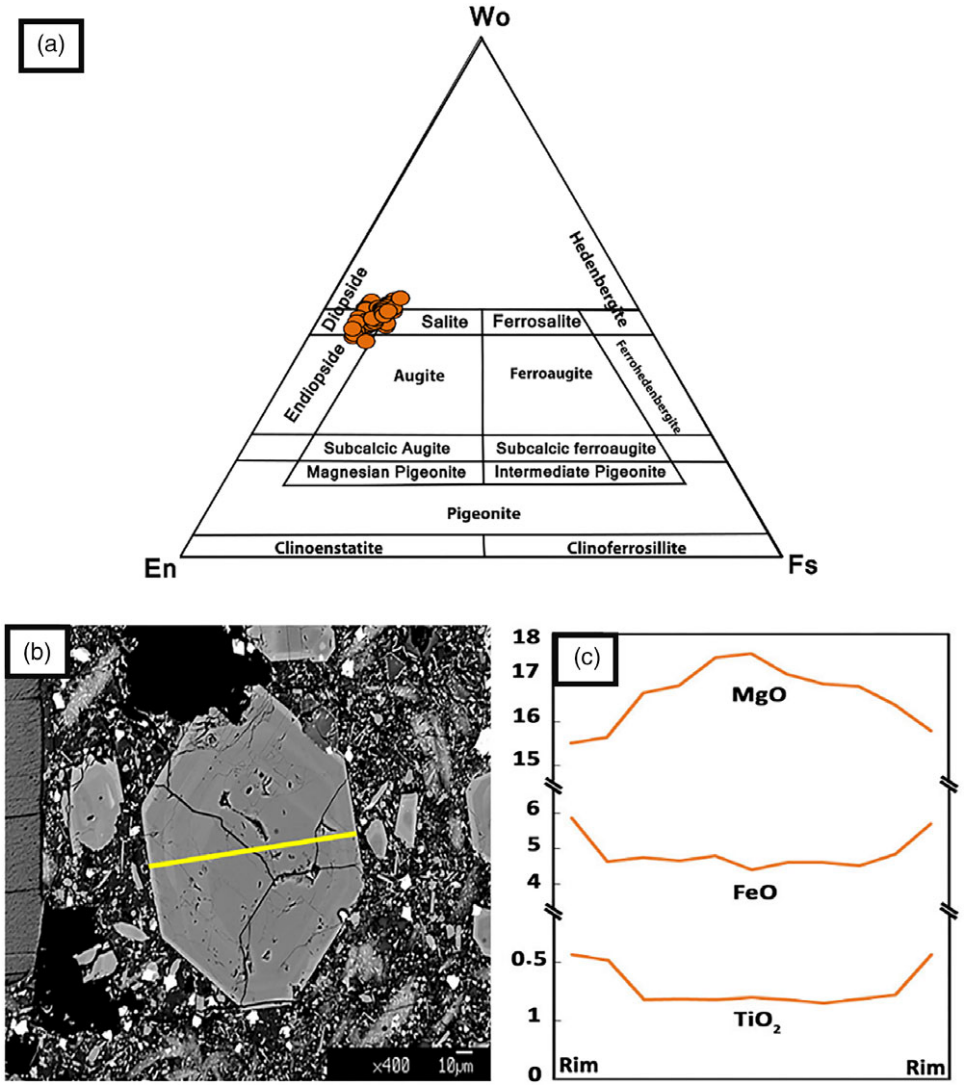

Fig. 5. (Colour online) (a) Classification scheme of Morimoto *et al.* (1988), showing that the pyroxenes are diopside–salite in composition; (b) backscattered electron image microphotograph of clinopyroxene from Illanlu (IL-C7); and (c) mineral compositional variation from rim to rim.

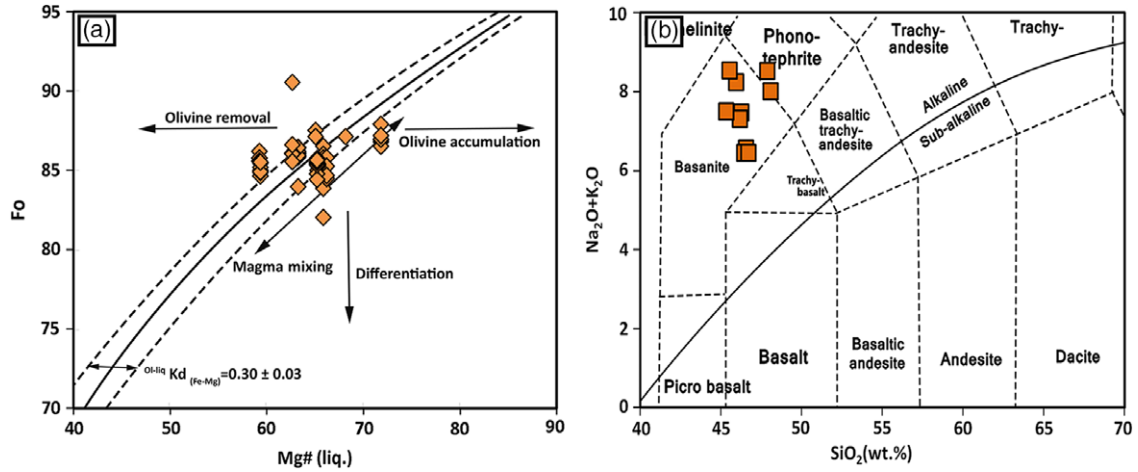

Fig. 6. (Colour online) (a) Variations of forsterite content in olivine vs Mg# of whole rock. Olivines in equilibrium with the host lavas plot between the dashed lines; (b) $Na_2O + K_2O$ (wt %) vs SiO_2 (wt %) diagram for the QBB rocks (Le Bas *et al.* 1986).

https://doi.org/10.1017/S0016756823000018 Published online by Cambridge University Press

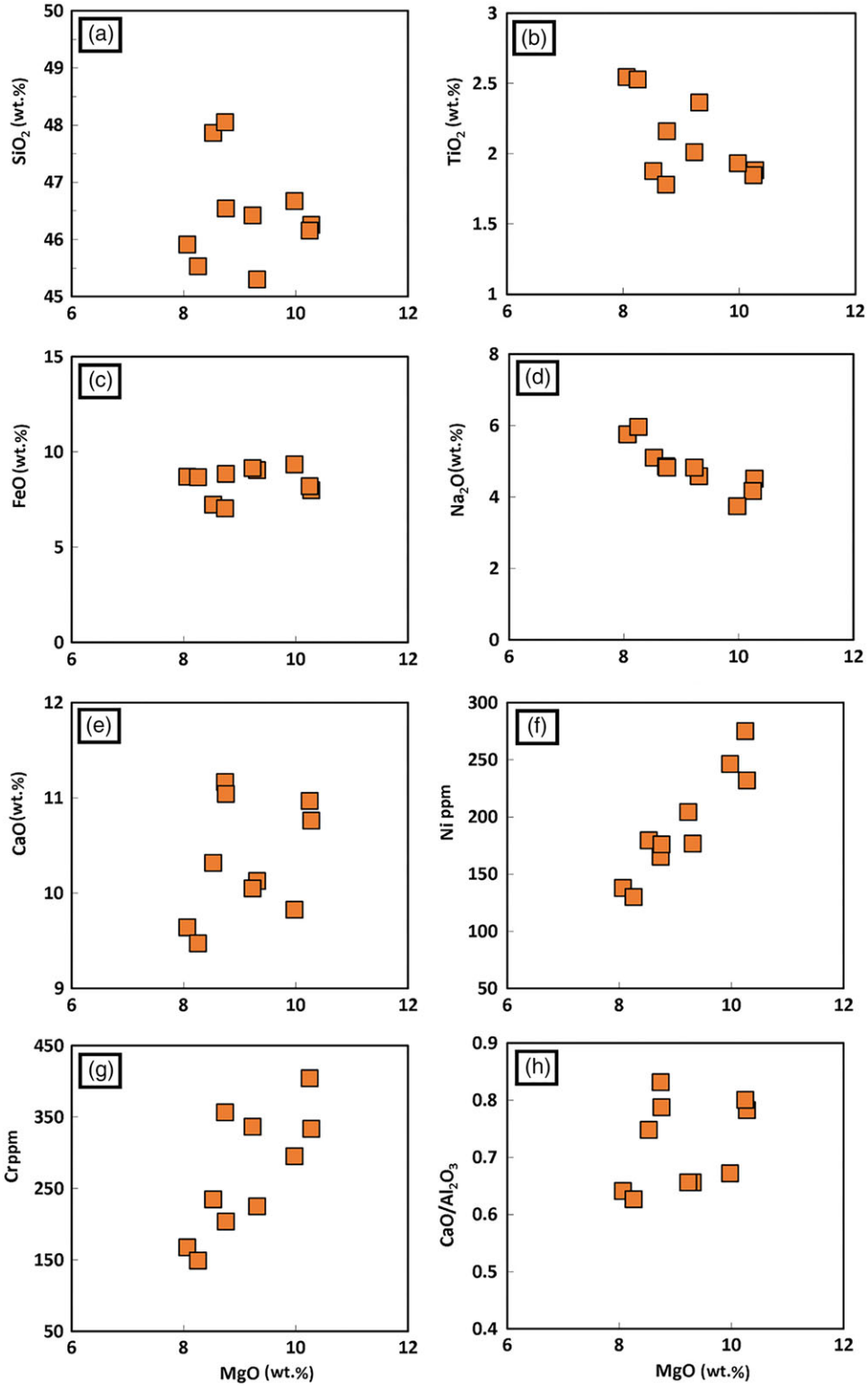

Fig. 7. (Colour online) Bivariate diagrams of selected major and trace elements against MgO (wt %).

ppm; Sr: 1586–3080 ppm; Pb: 11.2–28.1 ppm), and display negative Nb–Ta anomalies on primitive-mantle normalized abundance diagrams, which is a known characteristic of lavas derived from a mantle source with subduction-modified material or crustal contamination (Fig. 8b).

Whole-rock Nd–Sr isotopic analyses for QBB are reported in Table 1. Initial $^{87}Sr/^{86}Sr$ and $^{143}Nd/^{144}Nd$ ratios of QBB range from 0.70453 to 0.70535 and from 0.512643 to 0.512722 (ϵ_{Nd} +0.23 to +1.76), respectively. The QBB rocks plot close to the composition of the bulk silicate earth and have lower values of $^{87}Sr/^{86}Sr$ in

https://doi.org/10.1017/S0016756823000018 Published online by Cambridge University Press

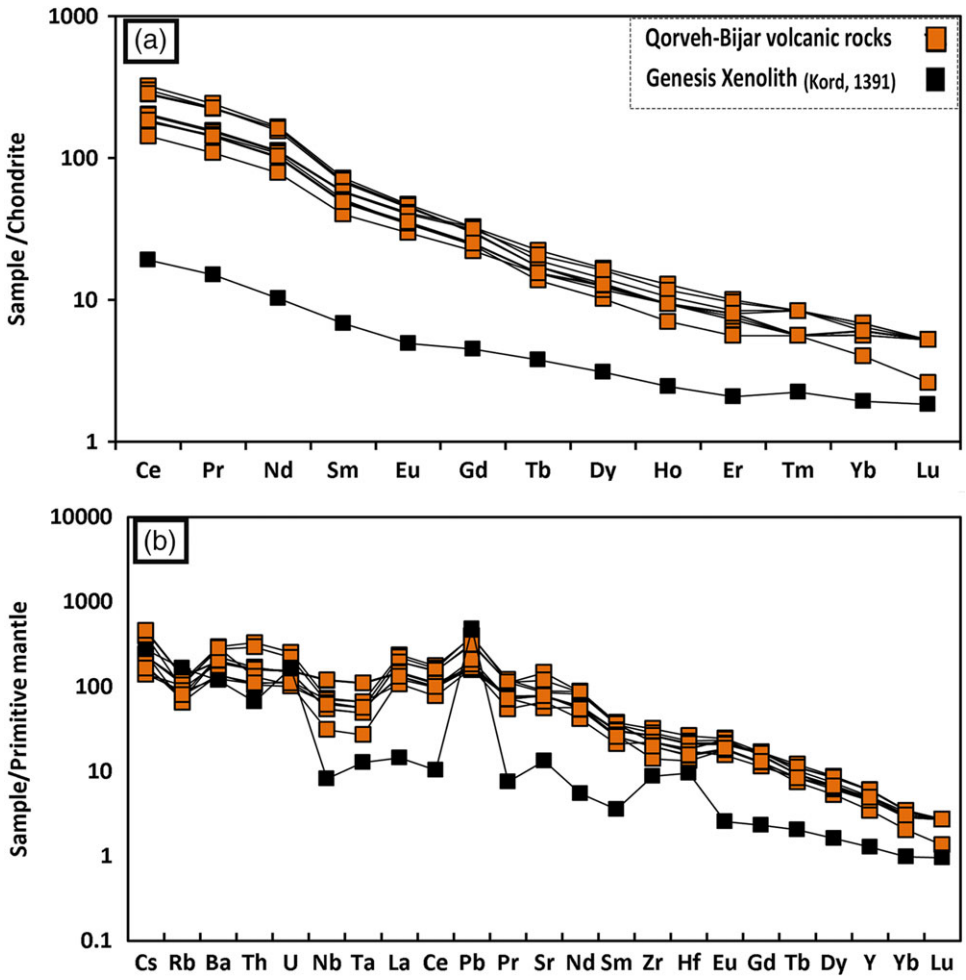

Fig. 8. (Colour online) (a) Chondrite-normalized REE diagram and (b) primitive-mantle-normalized trace element diagram for QBB rocks. Normalization values from Sun & McDonough (1989).

comparison to the gneissic xenoliths (Azizi *et al.* 2014) which are considered as continental crust components in the study area (Fig. 9a).

5.d. Intensive parameters

The pressure and temperature conditions of magmas were estimated using the clinopyroxene-melt based thermobarometric models of Putirka *et al.* (2003) and Putirka (2008), using as input data the compositions of the early-formed crystal cores and the whole-rock analyses (i.e. the original magma compositions). To ascertain whether the clinopyroxene-melt pairs were effectively in equilibrium at the time of crystallization, we employed the equilibrium test of Putirka (2008) based on Fe–Mg exchange between clinopyroxene core and whole rock (Fig. 9b). As seen in Figure 9b, values of $^{cpx\text{-}melt}Kd_{Fe-Mg}$ closely match, with both the equilibrium ranges of 0.27 ± 0.03 and 0.28 ± 0.08 indicated by Putirka *et al.* (2003) and Putirka (2008) (their eqs. 32a and 33), respectively. Calculations based on equilibrium clinopyroxene–melt pairs yield pressures and temperatures of 4–6 (±1.8) kbar and 1182–1213 (±27) °C, respectively (Table 2).

Olivine–melt equilibria are particularly useful for liquidus temperature estimates because the Fe–Mg exchange reaction is nearly constant over a wide range of temperature, bulk composition and oxygen fugacity (i.e. $^{Ol\text{-}melt}Kd_{Fe-Mg} = 0.30 \pm 0.03$), and because the olivine Fo content is highly sensitive to the thermal path of magma (e.g. Roeder & Emslie 1970; Kuritani *et al.* 2019; Rollinson 2019). Using the olivine-based thermometer approach of Putirka *et al.* (2007) (their eq. 4), we find that Fo_{85-87} olivine is in equilibrium with the whole-rock data (Fig. 6a), yielding crystallization onset temperatures of 1212–1264 (±27) °C.

6. Discussion

6.a. Fractional crystallization and crustal contamination

Post-melting processes including fractional crystallization and crustal contamination present challenges to deciphering trace element data to determine the nature and composition of the melt source region. We consider the QBB rocks with MgO >10 wt %, Ni ~300 ppm and Cr >400 ppm to be primary mantle melts. Ni, Cr and CaO contents decrease with decreasing MgO (Fig. 7f–g), consistent with minor fractionation of olivine, clinopyroxene and probably chromian spinel from parental magma. This interpretation is also supported by petrological observations.

Values of Eu/Eu* (0.9–1) and the lack of negative Eu anomalies in chondrite-normalized REE diagrams (Fig. 8) suggest that there is no significant plagioclase fractionation involved in the petrogenesis of the QBB rocks. Many QBB rocks have Ba and Sr abundances that record incompatible behaviour of these elements, consistent with olivine and clinopyroxene fractionation in the absence of plagioclase formation. Following Pang *et al.* (2012), the absence of negative correlations between Y or Sm, elements with comparatively higher Kd values for amphibole–liquid compared to

https://doi.org/10.1017/S0016756823000018 Published online by Cambridge University Press

Table 1. Rb–Sr and Sm–Nd isotopic data for the Qorveh–Bijar basaltic rocks

Samples*	$^{87}Rb/^{86}Sr$	±2s	$^{87}Sr/^{86}Sr$	$(^{87}Sr/^{86}Sr)_i$	$^{147}Sm/^{144}Nd$	±2s	$^{143}Nd/^{144}Nd$	$(^{143}Nd/^{144}Nd)_i$	ε_{Nd}
A2	0.1112	12	0.70528	0.70527	0.08649	9	0.51266	0.51266	0.43
A3	0.0928	10	0.70536	0.70535	0.08509	12	0.51265	0.51264	0.18
IL1	0.1088	11	0.7047	0.70469	0.10179	17	0.51271	0.5127	1.37
IL3	0.1272	13	0.70466	0.70465	0.10651	13	0.5127	0.51269	1.11
G1	0.0415	12	0.70489	0.70489	0.08318	12	0.51265	0.51265	0.23
G3	0.0411	11	0.70485	0.70485	0.08677	9	0.51266	0.51265	0.37
GH1	0.1609	11	0.70517	0.70515	0.09304	13	0.51267	0.51267	0.68
GH2	0.1158	17	0.70455	0.70453	0.09981	13	0.51273	0.51272	1.76
TE3	0.054	10	0.70465	0.70464	0.09369	13	0.51269	0.51269	1.03
TE4	0.0525	10	0.70469	0.70468	0.09423	13	0.51269	0.51269	1.07

*The age correction is based on the ages calculated by Boccaletti *et al.* (1976).

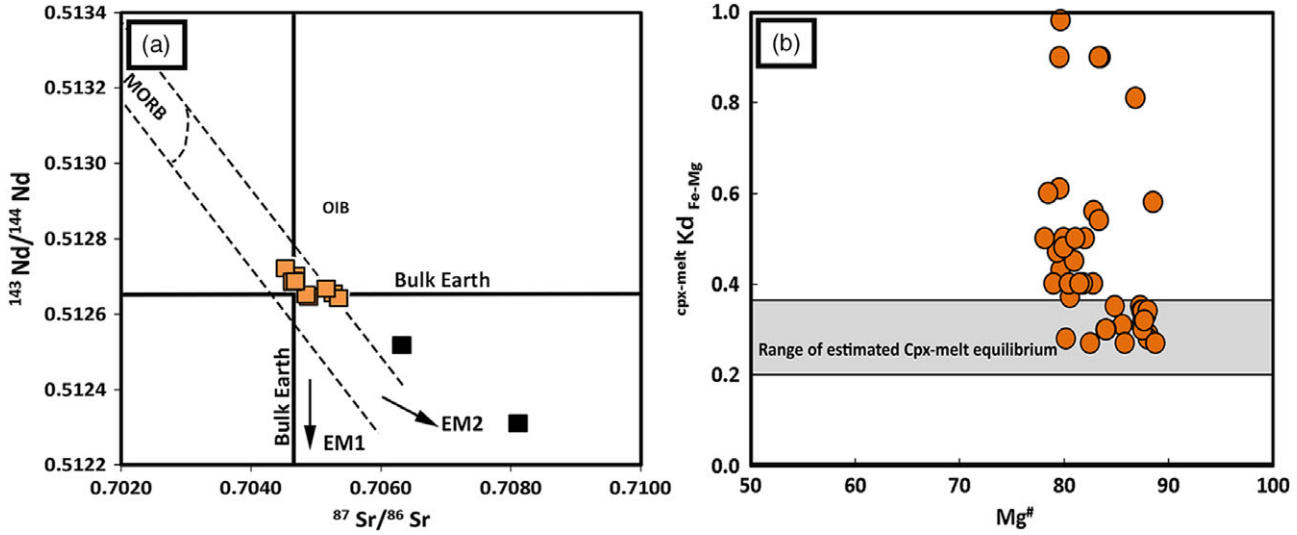

Fig. 9. (Colour online) (a) $^{87}Sr/^{86}Sr$ vs $^{143}Nd/^{144}Nd$. The compositions of Enriched Mantle 1 (EM1) and Enriched Mantle 2 (EM2) reservoirs come from Zindler & Hart (1986). The fields for OIBs and high-μ (HIMU) come from Hart (1988), and the composition of gneissic xenoliths comes from Azizi *et al.* (2014). (b) The Mg# of clinopyroxene is plotted against the value of $^{cpx\text{-}melt}Kd_{Fe\text{-}Mg}$ (Putirka *et al.* 2003; Putirka, 2008). Values of $^{cpx\text{-}melt}Kd_{Fe\text{-}Mg}$ closely match both the equilibrium ranges of 0.27 ± 0.03 and 0.28 ± 0.08 indicated by Putirka *et al.* (2003) and Putirka (2008), respectively.

pyroxene–liquid, and Cr (an index of fractionation) (Fig. 10a and b) indicates that amphibole fractionation was not substantial.

Before eruption, intra-plate basalts pass through thick continental crust, creating the possibility that they become contaminated by the crust. The QBB magmas had to pass through the thick continental lithosphere of western Iran (~110 km; Tunini *et al.* 2014), in which contamination may potentially occur. Indeed, the presence of abundant gneissic xenoliths provides evidence for this process. Numerous mantle xenoliths and xenocrysts are found in the study area; most of the xenoliths are fragmented in appearance with angular edges, suggesting that the host magma ascended too rapidly for them to melt, and thus too rapidly for crustal contamination to play a significant role in the petrogenesis of the QBB (Torkian *et al.* 2016; Salehi *et al.* 2020). The upper continental crust is characterized by enrichment in LILE, depletion in high-field-strength elements (HFSE), high SiO_2 (66.6 wt %; Rudnick *et al.* 2003) and enriched Sr–Nd isotopic compositions ($^{87}Sr/^{86}Sr = 0.7130$, ϵ_{Nd} −15; Gan *et al.* 2018). Consequently, magmas contaminated by continental material should be characterized by elevated SiO_2 and LILE concentrations as well as $^{87}Sr/^{86}Sr$ ratios, but lower HFSE concentrations and $^{143}Nd/^{144}Nd$ ratios. We emphasize that the QBB lava geochemistry does not display these key features. Further, the lack of systemic positive correlations in plots of Nb/Th – ϵ_{Nd} and Th/Yb – $^{87}Sr/^{86}Sr$ (Yu *et al.* 2020) implies negligible crustal contamination (Fig. 10c–d).

We employed FC–AFC–FCA® and mixing model software of Ersoy & Helvaci (2010) to investigate more fully the possible occurrence of crustal contamination; the model was constrained by the concentrations of incompatible trace elements Nb, Zr and Y in the mafic lavas and the original partition coefficients set in the model (Fig. 11). Primitive mafic lava GH2 with 45.3 wt % SiO_2 and 9.3 wt % MgO is assumed as the starting magma composition for AFC

https://doi.org/10.1017/S0016756823000018 Published online by Cambridge University Press

Table 2. Results from clinopyroxene-based thermobarometery, olivine-based thermometry for QBB rocks

	Clinopyroxene			Olivine	
	Putrika *et al.* (2003)	Putrika (2008)			Putrika *et al.* (2007)
Sample	*T* (°C)	*P* (kbar)	*T* (°C)	Fo content	*T* (°C)
Ghare-Toreh	1179	4.00	1182	87.5	1211
Illanlu	1236	5.00	1119	87.3	1264
Ahmad-Abad	1224	6.00	1213	85.5	1202
Tahmoures	1211	6.00	1186	85.2	1209
Ghale-Parian	1231	4.00	1213	84.9	1256

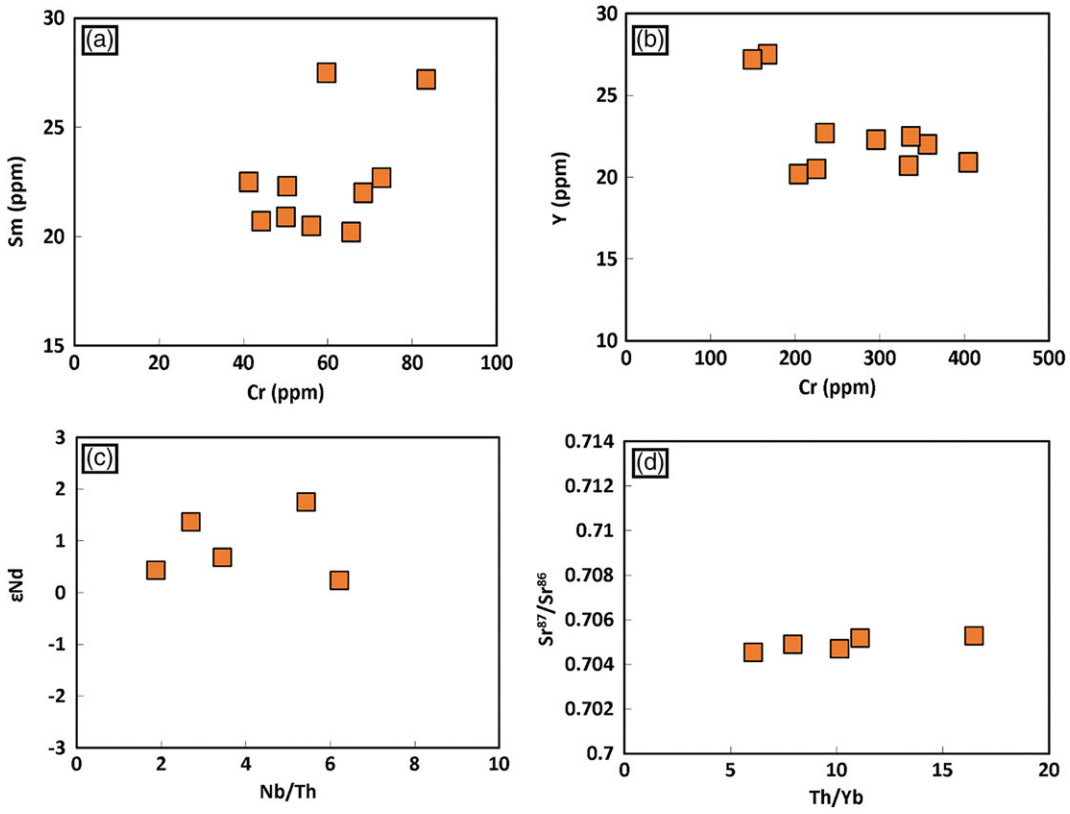

Fig. 10. (Colour online) (a) Y (ppm) vs Rb (ppm) and (b) Sm vs Rb diagrams for investigating the fractional crystallization for the QBB rocks; (c) Th/Yb vs $^{87}Sr/^{86}Sri$ and (d) Nb/Th vs ϵ_{Nd} for studied rocks.

modelling. The composition of the contaminant is that of gneissic xenolith sample EGH6 which contains Nb, Zr and Y 5.79 ppm, 98 ppm and 5.77 ppm, respectively (Kord, 2012). The investigated ratio of assimilation to fractionation (*r*) is 0.1, as higher *r* values would be inconsistent with the primitive MgO contents of the erupted products. Calculated model results plotted in the Zr/Y vs Nb diagram (Fig. 11a) essentially rule out the possibility that the geochemical signature of magmas is due to binary mixing with the continental crust or gneissic xenoliths. Rather, Nb enrichment results from its incompatibility in the fractionating phases of olivine and clinopyroxene. Correlations between $^{87}Sr/^{86}Sr$ vs Th and Nd^{143}/Nd^{144} vs Sr further support the trace element modelling, show a limited role for contamination (~5 %) and make it clear that the enriched nature of the QBB rocks could not result from crustal contamination (Fig. 11 b–c).

The primitive-mantle-normalized incompatible trace element abundance patterns of the QBB are characterized by negative anomalies in Nb and Ta which are a distinctive signature of subduction-related magmas (Wilson, 1989). Therefore, the simple mixing process between a primitive-mantle-derived magma and crustal material cannot be considered a viable mechanism to generate the observed trace element concentrations, and we must consider other factors such as enrichment of the mantle source by subduction components.

6.b. Mantle nature and modelling of melting

Distinguishing the source lithology is pivotal for interpreting the magmatic processes and origin of mantle-derived magmas. This identification can provide important constraints on crustal recycling and/or mantle metasomatism that may have contributed to mantle heterogeneity (Wang *et al.* 2012, 2014). Peridotites are abundant in the upper mantle, and the vast majority of Earth's basaltic lavas form through peridotite melting (Hirose &

https://doi.org/10.1017/S0016756823000018 Published online by Cambridge University Press

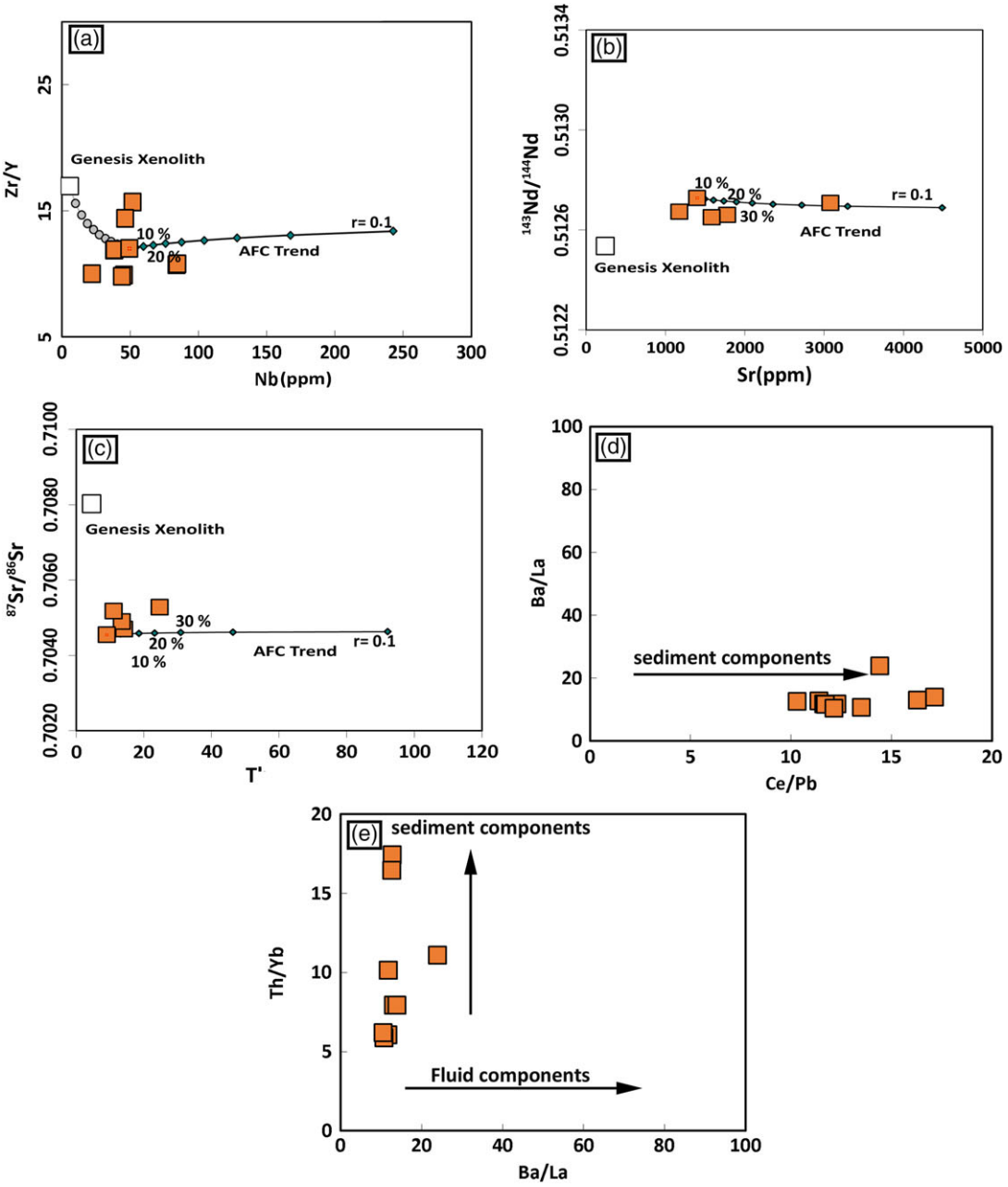

Fig. 11. (Colour online) Geochemical evidence for crustal contamination in Qorveh–Bijar lavas. (a) AFC modelling for the QBB rocks (gneissic xenoliths of Kord, 2012); (b) $^{143}Nd/^{144}Nd$ vs Sr (Moghadam *et al.* 2014); (c) $^{87}Sr/^{86}Sr$ vs Th (ppm) (Ersoy *et al.* 2012) with modelled assimilation – fractional crystallization pathways (AFC; $r = 0.4$ curve); (d) Ba/La vs Ce/Pb and (e) Th/Yb vs Ba/La plots to assess the effects of subducted slab materials on the mantle source of QBBs.

Kushiro, 1993; Walter, 1998; Rhodes *et al.* 2012). Experimental investigations, however, show that partial melts of volatile-free mantle peridotite are unable to match several important geochemical features of intra-plate basalts, including their TiO_2, CaO, FeO* and Al_2O_3 contents (Hirose & Kushiro, 1993; Hirschmann *et al.* 2003; Kogiso *et al.* 2003). As a result, intra-plate basalts have been suggested to be generated from pyroxenite, peridotite + CO_2, and hornblendite source lithologies (Pilet *et al.* 2008; Ying *et al.* 2013). The results of experimental studies illustrate that peridotite and pyroxenite may play a pivotal role in the genesis of basaltic magmas. The existence of pyroxenite in the mantle source of basaltic rocks can be discerned by comparing the major and trace elements chemistry of basaltic magmas with high-pressure experimental products (e.g. Hirschmann *et al.* 2003; Kogiso *et al.* 2003; Sobolev *et al.* 2007).

The incompatible element enrichment observed in the QBB rocks could be derived directly from an enriched mantle source (Fig. 8). However, the geodynamic history of the studiy area (SaSZ) leads us to investigate the possible occurrence of mantle metasomatism. It is accepted that slab-derived fluid or melts from ancient Neo-Tethyan oceanic slab subduction beneath the study area could affect the geochemical signature of the mantle source (Agard *et al.* 2011). The Ce/Pb ratio is sensitive to the proportion of sediment melt components: subducted sediments incorporated wholesale will increase Ce/Pb values of resulting lavas, whereas fluid components will decrease it because they are rich in fluid-

https://doi.org/10.1017/S0016756823000018 Published online by Cambridge University Press

mobile Pb (Tatsumi, 2000). We note that in the plot of Ba/La vs Ce/Pb (Fig. 11d), QBB rocks manifested the effects of sediment components in the mantle source. This is an excellent indicator of the type of sedimentary component because sediment-bound Pb is not mobilized by hydrous fluid, whereas it is incompatible during the melting of pelagic sediments (Class *et al.* 2000; Johnson & Plank, 2000). Moreover, high Th levels are commonly interpreted as reflecting the predominance of a component of subducted pelagic sediments in the magma source (Kirchenbaur *et al.* 2009; Kirchenbaur & Munker, 2015). The Th/Yb vs Ba/La plot shows that the QBB rocks array supports the involvement of melt components derived from sediments – but not fluids – during the enrichment of the mantle (Fig. 11e).

In addition to incorporating subducted sediments, the mantle source of the QBB experienced metasomatism by silicate melts. Clinopyroxenitic xenoliths have been reported in the Qorveh–Bijar basaltic rocks (Kord, 2012) and in Plio-Quaternary alkali basalts of the Marand area in NW Iran (Khezerlou *et al.* 2017). These samples provide valuable information on the nature and evolution of the lithospheric mantle in these areas (Downes, 1993; Griffin *et al.* 1999; Zhang *et al.* 2005; Nasir *et al.* 2006; Ackerman *et al.* 2012; Saadat & Stern, 2012; Ying *et al.* 2013).

Complex and diverse mechanisms have been proposed for the formation of pyroxenite veins or zones (Sobolev *et al.* 2007; Herzberg, 2011). Mantle pyroxenite can be generated by melting unmodified recycled basaltic crust (stage I pyroxenite) or by the reaction of melted subducted oceanic crust with solid peridotite (stage II pyroxenite; Sobolev *et al.* 2005). As the MgO content of QBB lavas (avg. MgO 9.2 wt %) are expected to be higher from melts of stage I pyroxenite (<8 wt % MgO; Pertermann & Hirschmann, 2003), we consider the melting of stage II pyroxenite. The experimental studies of Sobolev *et al.* (2005) show that eclogite has a lower solidus temperature than peridotite in the lithospheric mantle, therefore eclogite begins melting at higher pressures and greater depth. This melt has high Si concentration and can easily react with olivine-bearing peridotite, converting it to a solid olivine-free pyroxenite. Pyroxenites that result from silicate-melt-modified mantle are often considered the source of oceanic island and intercontinental basaltic rocks (Herzberg, 2006), and the geochemical characteristics of QBB lavas suggest it is the source of these eruptives.

Mafic melts derived from pyroxenite sources are geochemically distinguishable from melts originating from peridotite sources (Zeng *et al.* 2011; Sheldrick *et al.* 2020); these geochemical signatures are observed consistently in the QBB rocks and suggest contribution from a pyroxenite mantle source. First, melts of pyroxenite have lower CaO contents compared with peridotite-derived basaltic rocks of similar MgO content. While Ca is incompatible with olivine ($D_{CaO\ l} = 0.02$; Leeman & Scheidegger, 1977), the primary constituent of peridotite, it is compatible with clinopyroxene ($D_{CaCpx} = 1.8–2.0$; Pertermann & Hirschmann, 2002). As a result, the CaO content of pyroxenite melts will be lower than that of peridotite melts, as observed in the low CaO content of QBB lavas (Fig. 12a). Second, the QBB lavas have high Fe/Mn values which, following Kogiso & Hirschmann (2001) and Le Roux *et al.* (2010), can be attributed to pyroxenite melting (Fig. 12b). Finally, olivine-hosted melt inclusions in QBB mafic lavas manifest higher values of Zn/Fe*10000 than predicted for peridotite-derived melts, supporting a pyroxenite composition for the mantle source of the studied area (Salehi *et al.* 2020).

The QBB rocks show LREE enrichments counterbalanced by heavy REE (HREE) depletions; this strong fractionation effect (Fig. 8) suggests that garnet belongs to the phase assemblage of the mantle source (e.g. Coban, 2007). Y/Yb values >10 provide an additional clue that garnet is a residual phase in the source region (Ge *et al.* 2002). We note further that Nb concentrations (>20 ppm) and Nb/Ta values in the studied rocks are high (18–21), consistent with melting in the presence of rutile (Klemme *et al.* 2005; Liu *et al.* 2008).

We explore this question explicitly using Sm/Yb-La/Yb values to distinguish between melts formed in the garnet and spinel stability fields (Fig. 12e). Calculations are consistent with generation of the QBB volcanic rocks by a small degree (about 1 %) of partial melting from a garnet + rutile bearing pyroxenite source (Fig. 12e).

6.c. Geotectonic evolution

Several geological and geophysical studies attribute Iranian and East Anatolian magmatism to the break-off of the southern Neo-Tethyan oceanic slab beneath the Bitlis–Zagros suture and/or delamination of part of the lower lithosphere (e.g. Keskin, 2003; Şengör *et al.* 2003; Molinaro *et al.* 2005; Omrani *et al.* 2008; Hatzfeld & Molnar 2010; Agard *et al.* 2011; Chaharlang *et al.* 2020, Kettanah *et al.* 2021). Priestley and McKenzie (2006) suggest that lithosphere thickness in the study area is 150–200 km. Based on this inferred lithosphere thickness, Allen *et al.* (2013) rejected the process of delamination and suggested that the melting of amphibole- (richterite-)bearing mantle beneath the thickened lithosphere is responsible for the occurrence of melting in this region.

Fichtner *et al.* (2013) provide a very high-resolution tomographic model (~10–20 km) at crustal and lithospheric levels which highlights several low-velocity elliptical bodies (~100–150 km along the shortest axis and 200 km along the longest axis) beneath the study area. These bodies were named 'compaction pockets' by Soltanmohammadi *et al.* (2018), who suggested that they could be rising from the mantle transition zone. However, the model suggested by Salehi *et al.* (2020) raises the alternative that these bodies could be drips from the lithospheric mantle. Recent investigations by Motavalli-Anbaran *et al.* (2011) found that lithospheric thinning (100–120 km) affects the whole of the northern Zagros Mountains including central Iran, relative to a thickness of 180–200 km under the ZFTB and the Persian Gulf. Similarly, Tunini *et al.* (2014) identified abrupt thinning to *c.* 140 km under northwestern Iran including the QBB study area. Numerical studies of lithospheric drip and delamination indicate that even this moderate degree of abrupt lithospheric thinning is appropriate for the onset of drip melting. Geochemical modelling of REE abundances in the QBB rocks (Fig. 12d) suggests that the mantle source is garnet ± rutile bearing pyroxenite. Garnet-pyroxenite in the subcontinental lithospheric mantle will be denser than surrounding peridotite and hence gravitationally unstable, so it could delaminate locally and form a metasomatized drip (Elkins-Tanton, 2007). As this drip moves downwards it will undergo increased melting as it descends into the hot surrounding asthenosphere. This scenario is in marked contrast to adiabatic upwelling of the asthenosphere, where the degree of melting increases as the depth of melting shallows. The geochemical signature of the studied rocks supports the drip-melting model. Following Holbig & Grove (2008), covariation between the amount of normative olivine and Cr concentration in primitive mafic rocks can distinguish between the trends of adiabatic and drip melting (e.g. Furman *et al.* 2016; Gall *et al.* 2021). The QBB rocks follow

https://doi.org/10.1017/S0016756823000018 Published online by Cambridge University Press

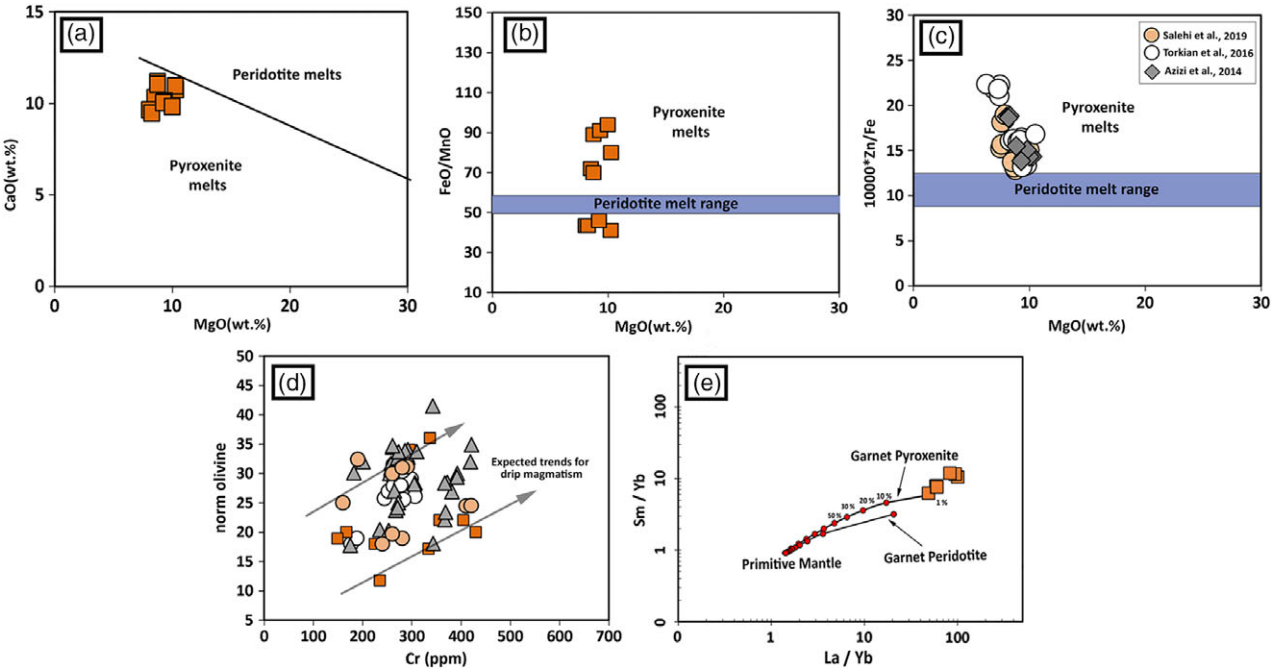

Fig. 12. (Colour online) (a–c) Bulk analyses of QBB mafic rocks display geochemical signatures consistent with melts of a pyroxenite mantle source. (d) Cr (ppm) (a proxy for melting degree) vs normative olivine content of mafic lavas (a proxy for melting pressure) diagram indicates lithospheric drip melting (e.g. Holbig & Grove 2008; Furman *et al*. 2016). Mafic lava sequences formed through adiabatic upwelling of asthenosphere define a negative correlation. (e) La/Yb vs Sm/Yb melt curves obtained using the non-modal batch melting equation of Shaw (1970) and mantle sources of both garnet-bearing pyroxenite ($Cpx_{60} + Grt_{40}$) and spinel-bearing peridotite ($Ol_{80} + Cpx_{16} + Grt_4$) (Kelemen *et al*. 2003; Pertermann *et al*. 2004). For both models, the values of C_0 come from the primitive-mantle data reported in Sun and McDonough (1989). The QBB rocks plot close to the garnet-bearing pyroxenite-melting curve with ~1 % of partial melting. Tick marks and numbers along the curves show the degree of partial melting for a given mantle source.

the trend for increased melting with depth as predicted for drip melting (Fig. 12e).

Edge convection along an abrupt lithospheric boundary can result in the melting of deep lithosphere that is suddenly exposed to heating; this process would develop analogous geochemical signatures in the melts. Undoubtedly, geochemical evidence is not enough to confirm lithospheric drip. However, the oval low-velocity zones could support the notion of partially molten zones within the lithospheric mantle. Their shape suggests they cannot ascend further as they are being compressed rather than rising from the asthenosphere, and we consider these oval-shaped low-velocity zones in the lithosphere to be pieces of foundered lithosphere, i.e., drips. Basaltic melts derived from these drips are likely to be rich in volatiles. They may ascend quickly to the surface along deep-rooted faults, allowing for only a brief stay in magma chambers where they would experience assimilation and fractional crystallization. Among the QBB samples, the low calculated degree of fractionation and the lack of plagioclase in the fractionating assemblage is consistent with this model rather than with a shallow chamber.

7. Conclusion

The Quaternary Qorveh–Bijar basaltic rocks (QBBs) located along a NW–SE trend parallel to the Zagros suture zone are typically alkali basalts with porphyritic, glomeroporphyritic and aphanitic textures. The main crystalline phases are olivine and clinopyroxene. The volcanic rocks show REE and LILE concentrations higher than those of the gneissic xenoliths they carry (which are assumed to represent the continental crust in the study area), indicating that geochemical variations within the QBB suite cannot be attributed to assimilation and/or mixing between primitive magmas and continental crust or gneissic material. High CaO contents, Fe/Mn and Zn/Fe values in the QBB lavas suggest that this mantle source is garnet-bearing pyroxenite in composition. As pyroxenite is denser than peridotitic lithospheric mantle, it is unstable gravitationally and can start to move downwards under its own weight through the process of mantle drip or localized delamination. This model is supported by geophysical data that confirmed the existence of elliptical-shaped low-velocity structures ~100–200 km in dimension interpreted as melt batches under the study area. Modelling of REE abundances (La/Yb and Sm/Yb) suggests the QBB lavas formed through low degrees of partial melting (~1 %) from an enriched mantle source in the garnet stability field. This source began to melt during descent in response to increasing temperatures, and the resulting magma ascended along deep-rooted faults, passing through a thick lithosphere where minor assimilation and fractional crystallization took place within the continental crust.

Supplementary material. To view supplementary material for this article, please visit https://doi.org/10.1017/S0016756823000018

Acknowledgements. This research was financially supported by the Bu-Ali Sina University (Iran) {T and S/1395}. The first author expresses her gratitude to the Ministry of Science and Technology of Iran and the Vice-Chancellor for Research and Technology of the Bu-Ali Sina University.

References

Ackerman L, Spacek P, Medaris Jr G, Hegner E, Svojtka M and Ulrych J (2012) Geochemistry and petrology of pyroxenite xenoliths from Cenozoic alkaline basalts, Bohemian Massif. *Journal of Geosciences* **57**, 199–219.

Agard P, Omrani J, Jolivet L, Whitechurch H, Vrielynck B, Spakman W, Monié P, Meyer B and Wortel R (2011) Zagros orogeny: a subduction-dominated process. *Geological Magazine* **148**, 692–725.

Alavi M (1994) Tectonics of the Zagros orogenic belt of Iran: new data and interpretations. *Tectonophysics* **229**, 211–38.

Allen MB, Kheirkhah M, Neill I, Emami MH and McLeod CL (2013) Generation of arc and within-plate chemical signatures in collision zone magmatism: Quaternary lavas from Kurdistan Province, Iran. *Journal of Petrology* **54**, 887–911.

Asan K and Kurt H (2011) Petrology and geochemistry of post-collisional early Miocene volcanism in the Karacadağ Area (Central Anatolia, Turkey). *Acta Geologica Sinica – English Edition* **85**, 1100–17.

Aydin F, Karsli O and Chen B (2008) Petrogenesis of the Neogene alkaline volcanics with implications for post-collisional lithospheric thinning of the Eastern Pontides, NE Turkey. *Lithos* **104**, 249–66.

Azizi H and Asahara Y (2013) Juvenile granite in the Sanandaj–Sirjan Zone, NW Iran: late Jurassic–early Cretaceous arc–continent collision. *International Geology Review* **55**, 1523–40.

Azizi H, Asahara Y and Tsuboi M (2014) Quaternary high-Nb basalts: existence of young oceanic crust under the Sanandaj–Sirjan Zone, NW Iran. *International Geology Review* **56**, 167–86.

Azizi H and Moinevaziri H (2009) Review of the tectonic setting of Cretaceous to Quaternary volcanism in northwestern Iran. *Journal of Geodynamics* **47**, 167–79.

Barber DE, Stockli DF, Horton BK, Koshnaw RI (2018) Cenozoic exhumation and foreland basin evolution of the Zagros orogen during the Arabia-Eurasia collision, western Iran. *Tectonics* **37**, 4396–420.

Berberian M and King GC (1981) Towards a palaeogeography and tectonics evolution of Iran. *Canadian Journal of Earth Sciences* **18**, 210–65.

Boccaletti M, Innocenti F, Manetti P, Mazzuoli R, Motamed A, Pasquare G, Radicati di Brozolo F and Amin Sobhani E (1976) Neogene and Quaternary volcanism of the Bijar Area (Western Iran). *Bulletin of Volcanology* **40**, 122–32.

Cebria JM, Lopez RJ, Doblas M, Oyarzun R, Hertogen J and Benito R (2000) Geochemistry of the Quaternary alkali basalts of Garrotxa (NE Volcanic Province, Spain); a case of double enrichment of the mantle lithosphere. *Journal of Volcanology and Geothermal Research* **102**, 217–35.

Chaharlang R, Ducea MN and Ghalamghash J (2020) Geochemical evidences for quantifying crustal thickness over time in the Urumieh-Dokhtar magmatic arc (Iran). *Lithos* **374**, 105723.

Class C, Miller DM, Goldstein SL and Langmuir CH (2000) Distinguishing melt and fluid subduction components in Umnak Volcanics, Aleutian Arc. *Geochemistry, Geophysics, Geosystems* **1**, 1–16.

Coban H (2007) Basalt magma genesis and fractionation in collision-and extension-related provinces: a comparison between eastern, central western Anatolia. *Earth-Science Reviews* **80**, 219–38.

Dewey JF, Pitman WC, Ryan WB and Bonnin J (1973) Plate tectonics and the evolution of the Alpine system. *Geological Society of America Bulletin* **84**, 3137–80.

Downes H (1993) The nature of the lower continental crust of Europe: petrological and geochemical evidence from xenoliths. *Physics of the Earth and Planetary Interiors* **79**, 195–218.

Ducea MN, Seclaman AC, Murray KE, Jianu D and Schoenbohm LM (2013) Mantle-drip magmatism beneath the Altiplano-Puna plateau, central Andes. *Geology* **41**, 915–18.

Eftekharnejad J (1981) Tectonic division of Iran with respect to sedimentary basins. *Journal of the Iranian Petroleum Society* **82**, 19–28 (in Persian).

Elkins-Tanton LT (2007) Continental magmatism, volatile recycling, and a heterogeneous mantle caused by lithospheric gravitational instabilities. *Journal of Geophysical Research* **21**, 98–112.

Emami MH, Sadeghi MMM and Omrani SJ (1993) *Magmatic map of Iran. Map of Iran 1:1,000,000*. Tehran: Geological Survey of Iran, internal report.

Ersoy Y and Helvaci C (2010) FC–AFC–FCA and mixing modeler: a Microsoft® Excel© spreadsheet program for modelling geochemical differentiation of magma by crystal fractionation, crustal assimilation and mixing. *Computers and Geosciences* **36**, 383–90.

Ersoy YE, Helvacı C, Uysal İ, Karaoğlu Ö, Palmer MR and Dindi F (2012) Petrogenesis of the Miocene volcanism along the İzmir-Balıkesir Transfer Zone in western Anatolia, Turkey: implications for origin and evolution of potassic volcanism in post-collisional areas. *Journal of Volcanology and Geothermal Research* **241**, 21–38.

Farmer GL, Glazner AF and Manley CR (2002) Did lithospheric delamination trigger late Cenozoic potassic volcanism in the southern Sierra Nevada, California? *Geological Society of America Bulletin* **114**, 754–68.

Fichtner A, Saygin E, Taymaz T, Cupillard P, Capdeville Y and Trampert J (2013) The deep structure of the North Anatolian fault zone. *Earth and Planetary Science Letters* **373**, 109–17.

Fitton JG and Dunlop HM (1985) The cameroon line, West Africa, and its bearing on the origin of oceanic and continental alkali basalt. *Earth and Planetary Science Letters* **72**, 23–38.

Furman T, Nelson WR and Elkins-Tanton LT (2016) Evolution of the East African rift: drip magmatism, lithospheric thinning and mafic volcanism. *Geochimica et Cosmochimica Acta* **185**, 418–34.

Gall H, Furman T, Hanan B, Kürkcüoğlu B, Sayit K, Yürür T, Sjoblom MP, Şen E and Şen P (2021) Post-delamination magmatism in south-central Anatolia. *Lithos* **399**, 106299.

Gan CS, Zhang YZ, Barry TL, He JW and Wang YJ (2018) Jurassic metasomatized lithospheric mantle beneath South China and its implications: geochemical and Sr-Nd isotope evidence from the late Jurassic shoshonitic rocks. *Lithos* **320**, 236–49.

Ge X, Li X, Chen Z and Li W (2002) Geochemistry and petrogenesis of Jurassic high Sr/Y low granitoids in eastern China: constraints on crustal thickness. *Chinese Science Bulletin* **47**, 962–80.

Ghasemi A and Talbot CJ (2006) A new tectonic scenario for the Sanandaj–Sirjan Zone (Iran). *Journal of Asian Earth Sciences* **26**, 683–93.

Griffin WL, Doyle BJ, Ryan CG, Pearson NJ, Suzanne YOR, Davies R, Kivi K, Van Achterbergh E and Natapov LM (1999) Layered mantle lithosphere in the Lac de Gras area, Slave craton: composition, structure and origin. *Journal of Petrology* **40**, 705–27.

Hart SR (1988) Heterogeneous mantle domains: signatures, genesis and mixing chronologies. *Earth and Planetary Science Letters* **90**, 273–96.

Hassanzadeh J and Wernicke BP (2016) The Neotethyan Sanandaj-Sirjan zone of Iran as an archetype for passive margin-arc transitions. *Tectonics* **35**, 586–621.

Hatzfeld D and Molnar P (2010) Comparisons of the kinematics and deep structures of the Zagros and Himalaya and of the Iranian and Tibetan plateaus and geodynamic implications. *Reviews of Geophysics* **48**, 1–48.

Herzberg C (2006) Petrology and thermal structure of the Hawaiian plume from Mauna Kea volcano. *Nature* **444**, 605–9.

Herzberg C (2011) Identification of source lithology in the Hawaiian and Canary Islands: implications for origins. *Journal of Petrology* **52**, 113–46.

Hirose K and Kushiro I (1993) Partial melting of dry peridotites at high pressures: determination of compositions of melts segregated from peridotite using aggregates of diamond. *Earth and Planetary Science Letters* **114**, 477–89.

Hirschmann MM, Kogiso T, Baker MB and Stolper EM (2003) Alkalic magmas generated by partial melting of garnet pyroxenite. *Geology* **31**, 481–4.

Holbig ES and Grove TL (2008) Mantle melting beneath the Tibetan Plateau: experimental constraints on ultra potassic magmatism. *Journal of Geophysical Research* **113**, 48–59.

Johnson MC and Plank T (2000) Dehydration and melting experiments constrain the fate of subducted sediments. *Geochemistry, Geophysics, Geosystems* **1**, 1–28.

Jung C, Jung S, Hoffer E and Berndt J (2006) Petrogenesis of Tertiary mafic alkaline magmas in the Hocheifel: Germany. *Journal of Petrology* **47**, 1637–71.

Kelemen PB, Rilling JL, Parmentier EM, Mehl L and Hacker BR (2003) Thermal structure due to solid-state flow in the mantle wedge beneath arcs. *Geophysical Monograph – American Geophysical Union* **138**, 293–311.

Keskin M (2003) Magma generation by slab steepening and breakoff beneath a subduction-accretion complex: an alternative model for collision-related volcanism in Eastern Anatolia, Turkey. *Geophysical Research Letters* **30**, 1–4.

Kettanah YA, Abdulrahman AS, Ismail SA, MacDonald DJ and Al Humadi H (2021) Petrography, mineralogy, and geochemistry of the Hemrin Basalt, Northern Iraq: implications for petrogenesis and geotectonics. *Lithos* **390**, 106109.

https://doi.org/10.1017/S0016756823000018 Published online by Cambridge University Press

Kheirkhah M and Mirnejad H (2014) Volcanism from an active continental collision zone: a case study on most recent lavas within Turkish-Iranian plateau. *Journal of Tethys* **2**, 81–92.

Khezerlou AA, Amel N, Gregoire M, Moayyed M and Jahangiri A (2017) Geochemistry and mineral chemistry of pyroxenite xenoliths and host volcanic alkaline rocks from North West of Marand (NW Iran). *Mineralogy and Petrology* **111**, 865–85.

Kirchenbaur A, Munker C and Marchev P (2009) The HFSE budget of post-collisional high-K basalts and shoshonites. *Geochimica et Cosmochimica Acta* **73**, 1417–65.

Kirchenbaur M and Munker C (2015) The behaviour of the extended HFSE group (Nb, Ta, Zr, Hf, W, Mo) during the petrogenesis of mafic K-rich lavas: the Eastern Mediterranean case. *Geochimica et Cosmochimica Acta* **165**, 178–99.

Klemme S, Prowatke S, Hametner K and Günther D (2005) Partitioning of trace elements between rutile and silicate melts: implications for subduction zones. *Geochimica et Cosmochimica Acta* **69**, 2361–71.

Kogarko LN (2006) Alkaline magmatism and enriched mantle reservoirs: mechanisms, time, and depth of formation. *Geochemistry International* **44**, 3–10.

Kogiso T and Hirschmann MM (2001) Experimental study of clinopyroxenite partial melting and the origin of ultra-calcic melt inclusions. *Contributions to Mineralogy and Petrology* **142**, 347–60.

Kogiso T and Hirschmann MM (2006) Partial melting experiments of bimineralic eclogite and the role of recycled mafic oceanic crust in the genesis of ocean island basalts. *Earth and Planetary Science Letters* **249**, 188–99.

Kogiso T, Hirschmann MM and Frost DJ (2003) High-pressure partial melting of garnet pyroxenite: possible mafic lithologies in the source of ocean island basalts. *Earth and Planetary Science Letters* **216**, 603–17.

Kord M (2012) *Study of ultramafic and gneissic enclaves in basaltic rocks, NE Qorveh, Kurdistan*. MSc thesis. Bu-Ali Sina University, Hamedan, Iran, 137 pp. Published thesis.

Kuritani T, Kimura JI, Miyamoto T, Wei H, Shimano T, Maeno F, Jin X and Taniguchi H (2009) Intraplate magmatism related to deceleration of upwelling asthenospheric mantle: implications from the Changbaishan shield basalts, northeast China. *Lithos* **112**, 247–58.

Kuritani T, Xia QK, Kimura JI, Liu J, Shimizu K, Ushikubo T, Zhao D, Nakagawa M and Yoshimura S (2019) Buoyant hydrous mantle plume from the mantle transition zone. *Scientific Reports* **9**, 1–7.

Kuritani T, Yokoyama T and Nakamura E (2008) Generation of rear-arc magmas induced by influx of slab-derived supercritical liquids: implications from alkali basalt lavas from Rishiri Volcano, Kurile arc. *Journal of Petrology* **49**, 1319–42.

Le Bas ML, Maitre RL, Streckeisen A and Zanettin B (1986) IUGS subcommission on the systematics of igneous rocks. A chemical classification of volcanic rocks based on the total alkali-silica diagram. *Journal of Petrology* **27**, 745–50.

Le Roux V, Lee CT and Turner SJ (2010) Zn/Fe systematics in mafic and ultramafic systems: implications for detecting major element heterogeneities in the Earth's mantle. *Geochimica et Cosmochimica Acta* **74**, 2779–96.

Lechmann A, Burg JP, Ulmer P, Guillong M and Faridi M (2018) Metasomatized mantle as the source of Mid-Miocene-Quaternary volcanism in NW-Iranian Azerbaijan: geochronological and geochemical evidence. *Lithos* **304**, 311–28.

Leeman WP and Scheidegger KF (1977) Olivine/liquid distribution coefficients and a test for crystal-liquid equilibrium. *Earth and Planetary Science Letters* **35**, 247–57.

Liu Y, Gao S, Kelemen PB and Xu W (2008) Recycled crust controls contrasting source compositions of Mesozoic and Cenozoic basalts in the North China craton. *Geochimica et Cosmochimica Acta* **72**, 2349–76.

Ma GS-K, Malpas J, Xenophontos C and Chan GH-N (2011) Petrogenesis of latest Miocene-Quaternary continental intraplate volcanism along the northern Dead Sea Fault System (Al Ghab-Homs volcanic field), western Syria: evidence for lithosphere-asthenosphere interaction. *Journal of Petrology* **52**, 401–30.

Malecootyan S, Hagh-Nazar S, Ghorbani M and Emami MH (2007) Magmatic evolution in Quaternary basaltic rocks in Ghorveh–Takab axis. *Journal of Geoscience* **16**, 166–78 (in Persian with English abstract).

Mansouri-Esfahani MM, Khalili M, Kochhar N and Gupta LN (2010) A-type granite of the Hasan Robat area (NW of Isfahan, Iran) and its tectonic significance. *Journal of Asian Earth Sciences* **37**, 207–18.

Míková J and Denková P (2007) Modified chromatographic separation scheme for Sr and Nd isotope analysis in geological silicate samples. *Journal of Geosciences* **52**, 221–6.

Moghadam HS, Ghorbani G, Khedr MZ, Fazlnia N, Chiaradia M, Eyuboglu Y, Santosh M, Francisco CG, Martinez ML, Gourgaud A and Arai S (2014) Late Miocene K-rich volcanism in the Eslamieh Peninsula (Saray), NW Iran: implications for geodynamic evolution of the Turkish–Iranian High Plateau. *Gondwana Research* **26**, 1028–50.

Mohajjel M and Fergusson CL (2014) Jurassic to Cenozoic tectonics of the Zagros Orogen in northwestern Iran. *International Geology Review* **56**, 263–87.

Moinevaziri H and Amin-Sobhani H (1988) *Study on Young Volcanoes of Qorveh-Takab Area*. Tehran: Tarbiat Moalem University Publications.

Molinaro M, Zeyen H and Laurencin X (2005) Lithospheric structure beneath the south-eastern Zagros Mountains, Iran: recent slab break-off? *Terra Nova* **17**, 1–6.

Morimoto N, Fabries J, Ferguson AK, Ginzburg IV, Ross M, Seifert FA and Zussman J (1988) Nomenclature of pyroxenes. *Mineralogical Magazine* **52**, 535–50.

Motavalli-Anbaran SH, Zeyen H, Brunet MF and Ardestani VE (2011) Crustal and lithospheric structure of the Alborz Mountains, Iran, and surrounding areas from integrated geophysical modelling. *Tectonics* **30**, 1–16.

Mouthereau F, Lacombe O and Vergés J (2012) Building the Zagros collisional orogen: timing, strain distribution and the dynamics of Arabia/Eurasia plate convergence. *Tectonophysics* **532**, 27–60.

Nasir S, Al-Sayigh A, Alharthy A and Al-Lazki A (2006) Geochemistry and petrology of tertiary volcanic rocks and related ultramafic xenoliths from the central and eastern Oman Mountains. *Lithos* **90**, 49–270.

Omrani J, Agard P, Whitechurch H, Benoit M, Prouteau G and Jolivet L (2008) Arc-magmatism and subduction history beneath the Zagros Mountains, Iran: a new report of adakites and geodynamic consequences. *Lithos* **106**, 380–98.

Pang KN, Chung S, Zarrinkoub MH, Khatib MM, Mohammadi SS, Chiu H, Chu CH, Lee H and Lo C (2013) Eocene–Oligocene post-collisional magmatism in the Lut–Sistan region, eastern Iran: magma genesis and tectonic implications. *Lithos* **180**, 234–51.

Pang KN, Chung SL, Zarrinkoub MH, Mohammadi SS, Yang HM, Chu CH, Lee HY and Lo CH (2012) Age, geochemical characteristics and petrogenesis of Late Cenozoic intraplate alkali basalts in the Lut–Sistan region, eastern Iran. *Chemical Geology* **306**, 40–53.

Pertermann M and Hirschmann MM (2002) Trace-element partitioning between vacancy-rich eclogitic clinopyroxene and silicate melt. *American Mineralogist* **87**, 1365–76.

Pertermann M and Hirschmann MM (2003) Partial melting experiments on a MORB-like pyroxenite between 2 and 3 GPa: Constraints on the presence of pyroxenite in basalt source regions from solidus location and melting rate. *Journal of Geophysical Research* **108**, 1–12.

Pertermann M, Hirschmann MM, Hametner K, Günther D and Schmidt MW (2004) Experimental determination of trace element partitioning between garnet and silica-rich liquid during anhydrous partial melting of MORB-like eclogite. *Geochemistry, Geophysics, and Geosystems* **5**, 2173–2201.

Pilet S, Baker MB and Stolper EM (2008) Metasomatized lithosphere and the origin of alkaline lavas. *Science* **320**, 916–19.

Pin C, Briot D, Bassin C and Poitrasson F (1994) Concomitant separation of strontium and samarium-neodymium for isotopic analysis in silicate samples, based on specific extraction chromatography. *Analytica Chimica Acta* **298**, 209–17.

Pin C and Zalduegui JS (1997) Sequential separation of light rare-earth elements, thorium and uranium by miniaturized extraction chromatography: application to isotopic analyses of silicate rocks. *Analytica Chimica Acta* **339**, 79–89.

Priestley K and McKenzie D (2006) The thermal structure of the lithosphere from shear wave velocities. *Earth and Planetary Science Letters* **244**, 285–301.

Putirka K, Perfit M, Ryerson FJ and Jackson MG (2007) Ambient and excess mantle temperatures, olivine thermometry, and active vs. passive upwelling. *Chemical Geology* **241**, 177–206.

Putirka KD (2008) Thermometers and barometers for volcanic systems. *Reviews in Mineralogy and Geochemistry* **69**, 61–120.

Putirka KD, Ryerson FJ and Mikaelian H (2003) New igneous thermobarometers for mafic and evolved lava compositions, based on clinopyroxene + liquid equilibria. *American Mineralogist* **88**, 1542–54.

Razavi MH and Sayyareh A (2010) Properties of young volcanic rocks in southeast of Bijar. *Journal of Geoscience* **19**, 151–6.

Rhodes JM, Huang S, Frey FA, Pringle M and Xu G (2012) Compositional diversity of Mauna Kea shield lavas recovered by the Hawaii Scientific Drilling Project: inferences on source lithology, magma supply, and the role of multiple volcanoes. *Geochemistry, Geophysics, Geosystems* **13**, 105747.

Roeder PL and Emslie R (1970) Olivine-liquid equilibrium. *Contributions to Mineralogy and Petrology* **29**, 275–89.

Rollinson H (2019) Dunites in the mantle section of the Oman ophiolite: the boninite connection. *Lithos* **334–335**, 1–7.

Rostami-Hossouri M, Ghasemi H, Pang KN, Shellnutt JG, Rezaei-Kahkhaei M, Miao L, Mobasheri M, Iizuka Y, Lee HY and Lin TH (2020) Geochemistry of continental alkali basalts in the Sabzevar region, northern Iran: implications for the role of pyroxenite in magma genesis. *Contributions to Mineralogy and Petrology* **175**, 1–22.

Rudnick RL, Gao S, Holland HD and Turekian KK (2003) Composition of the continental crust. *The Crust* **3**, 1–64.

Saadat S and Stern CR (2012) Petrochemistry of a xenolith-bearing Neogene alkali olivine basalt from north-eastern Iran. *Journal of Volcanology and Geothermal Research* **225**, 13–29.

Salehi N, Torkian A and Furman T (2020) Olivine-hosted melt inclusions in Pliocene–Quaternary lavas from the Qorveh–Bijar volcanic belt, western Iran: implications for source lithology and cooling history. *International Geology Review* **62**, 1828–44.

Şengör A, Ozeren S, Genc T and Zor E (2003) East Anatolian high plateau as a mantle-supported, north-south shortened domal structure. *Geophysical Research Letters* **30**, 1–24.

Şengör AMC and Kidd WSF (1979) Post-collisional tectonics of the Turkish-Iranian plateau and a comparison with Tibet. *Tectonophysics* **55**, 361–76.

Sepahi AA and Athari SF (2006) Petrology of major granitic plutons of the northwestern part of the Sanandaj-Sirjan Metamorphic Belt, Zagros Orogen, Iran: with emphasis on A-type granitoids from the SE Saqqez area. *Neues Jahrbuch für Mineralogie – Abhandlungen* **183**, 93–106.

Shahbazi H, Maghami YT, Azizi H, Asahara Y, Siebel W, Maanijou M and Rezai A (2021) Zircon U–Pb ages and petrogenesis of late Miocene adakitic rocks from the Sari Gunay gold deposit, NW Iran. *Geological Magazine* **158**, 1733–55.

Shahbazi H, Siebel W, Pourmoafee M, Ghorbani M, Sepahi AA, Shang CK and Abedini MV (2010) Geochemistry and U–Pb zircon geochronology of the Alvand plutonic complex in Sanandaj–Sirjan Zone (Iran): new evidence for Jurassic magmatism. *Journal of Asian Earth Sciences* **39**, 668–83.

Shaw DM (1970) Trace element fractionation during anataxis. *Geochimica et Cosmochimica Acta* **34**, 237–43.

Shaw JE, Baker JA, Menzies MA, Thirlwall MF and Ibrahim KM (2003) Petrogenesis of the largest intraplate volcanic field on the Arabian Plate (Jordan): a mixed lithosphere–asthenosphere source activated by lithospheric extension. *Journal of Petrology* **44**, 1657–79.

Sheldrick TC, Hahn G, Ducea MN, Stoica AM, Constenius K and Heizler M (2020) Peridotite versus pyroxenite input in Mongolian Mesozoic-Cenozoic lavas, and dykes. *Lithos* **376**, 105747.

Sobolev AV, Hofmann AW, Kuzmin DV, Yaxley GM, Arndt NT, Chung SL, Danyushevsky LV, Elliott T, Frey FA, Garcia MO and Gurenko AA (2007) The amount of recycled crust in sources of mantle-derived melts. *Science* **316**, 412–7.

Sobolev AV, Hofmann AW, Sobolev SV and Nikogosian IK (2005) An olivine-free mantle source of Hawaiian shield basalts: *Nature* **434**, 590–7.

Soltanmohammadi A, Grégoire M, Rabinowicz M, Gerbault M, Ceuleneer G, Rahgoshay M, Bystricky M and Benoit M (2018) Transport of volatile-rich melt from the mantle transition zone via compaction pockets: implications for mantle metasomatism and the origin of alkaline lavas in the Turkish–Iranian plate. *Journal of Petrology* **59**, 2273–310.

Stampfli GM and Borel GD (2002) A plate tectonic model for the Paleozoic and Mesozoic constrained by dynamic plate boundaries and restored synthetic oceanic isochrons. *Earth and Planetary Science Letters* **196**, 17–33.

Sun SS and McDonough QF (1989) Chemical and isotopic systematic of oceanic basalts; implications for mantle compositions and processes. In *Magmatism in the Ocean Basins* (eds AD Saunders and MJ Norry), pp. 312–45. Geological Society of London, Special Publication no. 42,.

Tatsumi Y (2000) Slab melting: its role in continental crust formation and mantle evolution. *Geophysical Research Letters* **27**, 3941–4.

Tavakoli N, Davoudian AR, Shabanian N, Azizi H, Neubauer F, Asahara Y and Bernroider M (2020) Zircon U-Pb dating, mineralogy and geochemical characteristics of the gabbro and gabbro-diorite bodies, Boein–Miandasht, western Iran. *International Geology Review* **62**, 1658–76.

Temel A, Gourgaud A, Alıcı P and Bellon H (2000) The role of asthenospheric mantle in the generation of Tertiary basaltic alkaline volcanism in the Polatlı – Ankara region, central Anatolia, Turkey: constraints from major-element, traceelement and Sr–Nd isotopes, Goldschmidt 2000, September 3–8th. *Journal of Conference Abstracts* **5**, 989.

Temel A, Yürür T, Alıcı P, Varol E, Gourgaud A, Bellon H and Demirbağ H (2010) Alkaline series related to Early-Middle Miocene intra-continental rifting in a collision zone: an example from Polatlı, Central Anatolia, Turkey. *Journal of Asian Earth Sciences* **38**, 289–306.

Thompson RN and Gibson SA (2000) Transient high temperatures in mantle plume heads inferred from magnesian olivines in Phanerozoic picrites. *Nature* **407**, 502–6.

Thompson RN, Ottley CJ, Smith PM, Pearson DG, Dickin AP, Morrison MA, Let PT and Gibson SA (2005) Source of the Quaternary alkalic basalts, picrites and basanites of the Potrillo Volcanic Field, New Mexico, USA: lithosphere or convecting mantle? *Journal of Petrology* **46**, 1603–43.

Torkian A and Furman T (2015) The significance of mafic microgranular enclaves in the petrogenesis of the Qorveh Granitoid Complex, northern Sanandaj-Sirjan Zone, Iran. *Neues Jahrbuch für Mineralogie – Abhandlungen* **192**, 117–33.

Torkian A, Furman T, Salehi N and Veloski K (2019) Petrogenesis of adakites from the Sheyda volcano, NW Iran. *Journal of African Earth Sciences* **150**, 194–204.

Torkian A, Salehi N and Sieble W (2016) Geochemistry and petrology of basaltic lavas from NE-Qorveh, Kurdistan province, Western Iran. *Journal of Mineral Chemistry* **193**, 95–112.

Tunini L, Jimenez-Munt I, Fernandez M, Verges J and Villasenor A (2014) Lithospheric mantle heterogeneities beneath the Zagros Mountains and the Iranian Plateau: a petrological-geophysical study. *Geophysical Journal International* **200**, 596–614.

Verma SP and Molaei-Yeganeh T (2022) Tectonic settings of the Plio-Quaternary volcanism in Iran from multidimensional and multielement solutions. *Geological Journal* **57**, 410–24.

Walter MJ (1998) Melting of garnet peridotite and the origin of komatiite and depleted lithosphere. *Journal of Petrology* **39**, 29–60.

Wang XC, Li ZX, Li J, Pisarevsky SA and Wingate MT (2014) Genesis of the 1.21 Ga Marnda Moorn large igneous province by plume–lithosphere interaction. *Precambrian Research* **241**, 85–103.

Wang XC, Li ZX, Li XH, Li J, Liu Y, Long WG, Zhou JB and Wang F (2012) Temperature, pressure, and composition of the mantle source region of Late Cenozoic basalts in Hainan Island, SE Asia: a consequence of a young thermal mantle plume close to subduction zones?. *Journal of Petrology* **53**, 177–233.

Wilson M (1989) *Igneous Petrogenesis*. London: Unwin Hyman, 466 pp.

Wilson M and Patterson R (2001) Intra-plate magmatism related to hot fingers in the upper mantle: evidence from the Tertiary-Quaternary volcanic province of western and central Europe. In*Mantle Plumes: Their Identification through Time* (eds R Ernst and K Buchan), pp. 37–58. Geological Society of America Special Paper 352.

Xu YG, Ma JL, Frey FA, Feigenson MD and Liu JF (2005) Role of lithosphere–asthenosphere interaction in the genesis of Quaternary alkali and tholeiitic basalts from Datong, western North China Craton. *Chemical Geology* **224**, 247–71.

https://doi.org/10.1017/S0016756823000018 Published online by Cambridge University Press

Yeganeh TM, Torkian A, Christiansen EH and Sepahi AA (2018) Petrogenesis of the Darvazeh mafic-intermediate intrusive bodies, Qorveh, Sanandaj-Sirjan zone, Iran. *Arabian Journal of Geosciences* **11**, 1–20.

Ying J, Zhang H, Tang Y, Su B and Zhou X (2013) Diverse crustal components in pyroxenite xenoliths from Junan, Sulu orogenic belt: implications for lithospheric modification invoked by continental subduction: *Chemical Geology* **356**, 181–92.

Yu SY, Chen LM, Lan JB, He YS, Chen Q and Song XY (2020) Controls of mantle source and condition of melt extraction on generation of the picritic lavas from the Emeishan large igneous province, SW China. *Journal of Asian Earth Sciences* **203**, 104534.

Zeng G, Chen L-H, Xu X-S, Jiang S-Y and Hofmann AW (2010) Carbonated mantle sources for Cenozoic intra-plate alkaline basalts in Shandong, North China. *Chemical Geology* **273**, 35–45.

Zeng G, Chen LH, Hofmann AW, Jiang SY and Xu XS (2011) Crust recycling in the sources of two parallel volcanic chains in Shandong, North China. *Earth and Planetary Science Letters* **302**, 359–68.

Zhang SQ, Mahoney JJ, Mo XX, Ghazi AM, Milani L, Crawford AJ, Guo TY and Zhao ZD (2005) Evidence for a widespread Tethyan upper mantle with Indian-Ocean-Type isotopic characteristics. *Journal of Petrology* **46**, 29–58.

Zindler A and Hart S (1986) Chemical geodynamics: *Earth and Planetary Science* **14**, 493–571.

Zou H, Zindler A, Xu X and Qi Q (2000) Major, trace element, and Nd, Sr and Pb isotope studies of Cenozoic basalts in SE China: mantle sources, regional variations, and tectonic significance. *Chemical Geology* **171**, 33–47.

https://doi.org/10.1017/S0016756823000018 Published online by Cambridge University Press